1 **Impact of Clouds and Aerosols on Photolysis Frequencies and Photochemistry during**

2 **TRACE-P, Part I: Analysis using Radiative Transfer and Photochemical Box Models**

3 B.L. Lefer[1], R.E. Shetter[1], S.R. Hall[1], J.H. Crawford[2], and J.R. Olson[2]

4 [1] National Center for Atmospheric Research, Boulder, CO 80305
5 [2] NASA Langley Research Center, Hampton, VA, 23681

1   **Abstract.** This study examines the agreement between photolysis frequency measurements by

2   the NCAR scanning actinic flux spectroradiometer (SAFS) and calculations from a cloud-free

3   model (CFM) and investigates the impact of these differences on ozone photochemistry.

4   Overall, the mean $j\text{NO}_2$ measurement to model ratio for all flights of TRACE-P was

5   0.943±0.271. The sky conditions during the TRAnsport and Chemical Evolution over the Pacific

6   (TRACE-P) experiment were determined to be "cloud-free" 40% of the time; hence, a CFM is

7   frequently not representative of the local atmospheric conditions. Our analysis indicates that

8   clouds have a larger impact on photolysis frequencies (from –90 to +200%) than do aerosols

9   (maximum of ±20%). The CFM and SAFS $j\text{NO}_2$ and $j\text{O}(^1\text{D})$ values differed by 9% and 0-7%,

10   respectively, during a vertical profile through a cloud-free and low AOD atmosphere. This

11   suggests that measurement/model agreement to less than 10% may be difficult without better

12   aerosol optical parameter inputs even under low-AOD conditions. For the TRACE-P chemical

13   environment, OH, NO, and HO_2 were more sensitive than other compounds (e.g., $\text{CH}_3\text{C(O)O}_2$,

14   CH_3OOH) to changes (or errors) in photolysis frequency inputs to a photochemical box model.

15   Compounds including NO_2, PAN and HCHO exhibited different relationships to j-value changes

16   below and above the boundary layer. Ozone production and loss rates increased linearly with

17   changes (or errors) in the photolysis frequency with the resulting net O_3 tendency increasing with

18   a linear slope near unity. During the TRACE-P mission, the net photochemical effect of clouds

19   and aerosols was a large decrease in photochemical O_3 production in the boundary layer.

20

1. Introduction

Atmospheric chemistry is strongly driven by the photolysis of trace gases resulting in the production of highly reactive radicals and direct and indirect removal of many chemical species. As solar UV radiation is transmitted through the atmosphere it is scattered and absorbed by gas molecules, cloud droplets, and aerosol particles. Consequently, clouds and aerosols can both reduce and enhance the UV actinic flux depending on their optical properties, solar zenith angle, and the position of the layer of interest relative to the observation point.

The impact of clouds on actinic radiation and photochemistry has been studied previously [*Thompson*, 1984; *Madronich*, 1987; *van Weele and Duynkerke*, 1993]; however, the recent availability of high-quality measurements of actinic flux and photolysis frequencies has resulted in a closer examination of radiative transfer in a cloudy atmosphere [e.g., *Crawford et al.*, 1999a; *Früh et al.*, 2000; *Pfister et al.*, 2000; *Junkermann et al.*, 2002; *Shetter et al.*, 2002]. Recent studies have shown that the cloud reduction of solar radiation is wavelength-dependent in the UV-range with the longer wavelength UV-A radiation being more strongly attenuated than the UV-B wavelengths [e.g., *Seckmeyer et al.*, 1996; *Crawford et al.*, 2002]. While reduced photolysis frequencies occur underneath a cloud, aircraft measurements have shown that the UV radiation reflected up from the cloud can enhance the upwelling actinic flux by 50% to 150%, resulting in a 30-40% increase in the total above-cloud photolysis frequency [e.g., *Shetter and Müller*, 1999; *Pfister et al.*, 2000]. Model calculations by *Madronich* [1987] predicted actinic flux enhancements of 2-3 times within the top layers of a cloud. Increases in actinic radiation on the order of 200% were later observed in stratocumulus clouds by *Vilà-Guerau de Arellano et al.* [1994]. In addition, short-term local enhancement of photolysis frequencies (by as much as 40%) has been observed at the Earth's surface under some specific broken-cloud conditions

1   where the disk of the sun is not occluded by a cloud and the cloudy portion of the sky is brighter

2   than the clear-sky portion [e.g., *Nack and Green*, 1974; *Lantz et al.*, 1996].

3   The change in UV radiation due to aerosols [e.g., *Liu et al*., 1991; *Ma and Guicherit*,

4   1997; *Papayannis et al.*, 1998; *Hofzumahaus et al.*, 2002; *Schafer et al.*, 2002] and the effects of

5   aerosols on photolysis frequencies [*Lantz et al.*, 1996; *Reuder and Schwander*, 1999; *Dickerson*

6   *et al*., 1997; *Jacobson*, 1998; *He and Carmichael*, 1999; *Liao et al.*, 1999; *Castro et al*., 2001;

7   *Balis et al.*, 2002] have also been investigated recently. In highly polluted conditions,

8   *Papayannis et al*. [1998] measured a 30% reduction in the UV-B radiation reaching the Earth's

9   surface due to aerosols. Absorbing aerosols reduce the UV actinic flux throughout the boundary

10   layer [e.g., *Wendisch et al.*, 1996] and as a result decrease near-surface photochemical ozone

11   production [*Dickerson et al.*, 1997; *Jacobson*, 1998]. Estimates of the reduction in ground-level

12   ozone caused by absorbing aerosols range from 5-7% for Los Angeles [Jacobson, 1998] to 70%

13   in an urban environment with a large aerosol loading [*He and Carmichael*, 1999]. Model

14   simulations have predicted that strongly scattering aerosols in the boundary layer result in an

15   increase in photolysis frequencies throughout the troposphere, increasing lower tropospheric

16   ozone mixing ratios in the eastern United States by 5 to 60% (20 to 45 ppbv) [*Dickerson et al*.,

17   1997, *He and Carmichael*, 1999]. *Liao et al*. [1999] examined aerosol impacts on photolysis

18   frequencies and determined that the increase in actinic flux due to scattering aerosols is

19   diminished in the presence of clouds while the reductions in photolysis frequencies due to

20   absorbing aerosols are further accentuated by interactions with a cloud layer.

21   The objectives of the TRACE-P (TRAnsport and Chemical Evolution over the Pacific)

22   mission (February - April 2001) were to examine the pathways for outflow of chemically and

23   radiatively important gases and aerosols and their precursors, from eastern Asia to the western

1 Pacific, and to determine the chemical evolution of the Asian outflow over the western Pacific

2 (refer to Jacob et al., [2003] for a summary of the TRACE-P scientific results). To better

3 quantify the radiative effects of clouds and aerosols on atmospheric chemistry, an improved

4 understanding of how clouds and aerosols impact the atmospheric profiles of photolysis

5 frequencies is necessary. The photolysis frequency measurements aboard the NASA DC-8 (20

6 flights) and P-3B (24 flights) aircraft during TRACE-P provided an opportunity to examine these

7 measurements over a range of altitudes and solar zenith angles in clear and cloudy skies with

8 urban and remote aerosol conditions. As such, this is the first half of a two-part study to

9 investigate the impacts of clouds and aerosol on photolysis frequencies and photochemistry. The

10 goal of Part I is to examine the agreement between photolysis frequencies derived from TRACE-

11 P measurements and from a detailed 1-D radiative transfer model and to explore the degree to

12 which these changes in UV radiation impacted the instantaneous ozone photochemistry as

13 determined by a 0-D photochemical box model. In Part II, Tang et al. [2003], will examine how

14 well a three-dimensional regional chemical transport model, STEM, coupled with a detailed

15 radiation model represents the cloud and aerosol optical conditions encountered during TRACE-

16 P. The broader-scale impacts of clouds and aerosols on photochemistry will also be investigated

17 in the second paper by comparing the chemical outputs from the full cloud and aerosol case to

18 "no aerosol" and "no cloud and no aerosol" assumptions.

19 **2. Methods**

20 **2.1 SAFS Instrumentation**

21 The scanning actinic flux spectroradiometer (SAFS) instrumentation on both the DC-8

22 and P-3B aircraft consisted of two identical (zenith and nadir) automated spectroradiometers,

23 each collecting radiation from one hemisphere (2π sr). These instruments are described in

1   *Shetter and Müller* [1999], with improvements to the instruments described in *Shetter et al.*,

2   [2002]. The SAFS instrument was previously deployed on both the NASA P-3B and DC-8

3   aircraft during PEM-Tropics B (refer to *Lefer et al.* [2001] for more details regarding the

4   instrument installation on these aircraft). The SAFS instrument measurements were compared

5   with several jNO_2 filter radiometers [*Lefer et al.*, 2001; *Shetter et al.*, 2003] and two different

6   actinic flux spectroradiometer systems [*Cantrell et al.*, 2003*; Shetter et al.*, 2003; *Bais et al.*,

7   2003] during the 1998 International Photolysis Frequency Measurement and Modeling

8   Intercomparison (IPMMI) campaign in Marshall, Colorado. Some results are discussed in

9   section 2.3.

10   Briefly, the main components of each SAFS instrument are an optical collector, a custom

11 UV fiber optic bundle, a computer-controllable double monochromator, a select low-dark current

12 photomultiplier tube, a custom four-channel signal amplifier, and a rack mount data acquisition

13 and control system. The monochromator, photomultiplier tube, and amplifier are temperature-

14 stabilized at 312 K. The full-width at half maximum of the CVI CM112 double monochromator

15 used in this instrument is 1.0 nm using 2400-g/mm gratings and 600-micron entrance and exit

16 slits. The acquisition time for a 280 nm to 422 nm spectrum is 10 seconds. The separate zenith

17 and nadir SAFS systems are synchronized to within 1 millisecond to assure simultaneous reading

18 at each wavelength in a spectrum.

19   The monochromator wavelength assignment and instrument function were checked

20 before each flight by referencing to a low-pressure mercury lamp spectrum. The absolute

21 spectral sensitivity of each instrument is calibrated in an optical calibration facility using 1000-

22 watt NIST traceable quartz-tungsten-halogen lamps with uncertainties of 3-4%. These primary

23 laboratory calibrations were performed before shipment for aircraft integration and after the

1   instruments returned from the field. In order to trace any drift in instrument sensitivity, spectral

2   calibrations were also performed in the field before each flight, using secondary 250-watt QTH

3   calibration lamps mounted in a field calibration unit. A thorough uncertainty analysis of the

4   SAFS instrument is discussed in *Shetter et al*. [2002]. During TRACE-P, the accuracy of the

5   actinic flux measured by the spectroradiometers was estimated to be between 6 % in the UV-B

6   and 5 % in the UV-A range. The precision of these measurements was between 3 % in the UV-B

7   and 2 % in the UV-A range. Overall, the instruments performed well and returned > 85% data

8   coverage for both aircraft.

9   **2.2 Cloud-Free Radiative Transfer Model (CFM)**

10   The Tropospheric Ultraviolet-Visible (TUV) model version 4.1 (publicly available at

11   http://www.acd.ucar.edu/TUV/) was used to calculate an *in situ* spectral actinic flux along the

12   aircraft flight tracks. TUV has been previously described by Madronich and Flocke [1999].

13   Briefly, the model considers the solar spectral irradiance incident at the top of the Earth's

14   atmosphere (van Hoosier et al., 1987; Neckel and Labs, 1984) and calculates the propagation of

15   this radiation as it passes through the atmosphere. The radiation field is modified by Rayleigh

16   and Mie scattering and absorption due to various gases and particles, as well as Lambertian

17   reflection at the surface. Gaseous absorbers include O_2 and O_3, as well as SO_2 and NO_2, if these

18   are present in substantial amounts (e.g., urban atmospheres). Aerosols can absorb or scatter

19   (Mie) radiation, depending on size and chemical composition. To account for the vertical

20   variations of atmospheric constituents, the model, in our implementation, subdivides the

21   atmospheric into 150 vertical layers of 100-meter vertical thickness from 0 to 15 kilometers and

22   85 vertical layers of 1-kilometer vertical thickness from 15 to 100 kilometers. In this application

23   we employ an eight-stream discrete ordinates scheme radiation solver. This calculation is

1   repeated at each wavelength between 280-422 nm with a spectral resolution of 1 nm. The model

2   computes, for each altitude and each wavelength, the spectral actinic fluxes associated with the

3   direct solar beam and the downwelling and upwelling diffuse radiation fields. The TUV model

4   was compared to other photochemical radiative transfer codes during the IPMMI campaign

5   [*Shetter et al.*, 2003; *Bais et al.*, 2003]. Some results are discussed in section 2.3.

6   In this study, this version of TUV was run for every 10 seconds of each TRACE-P flight

7   at the latitude, longitude, and altitude of the aircraft (> 100,000 data points). Standard model

8   conditions consisted of cloud-free skies, vertical profiles of air, O_3, temperature from the *U.S.*

9   *Standard Atmosphere* [1976], and a wavelength-independent surface albedo of 10% for ocean

10   [*Madronich*, 1993] and 5% for the few portions of TRACE-P flights over land [Feister and

11   Grewe, 1995]. The TOMS O_3 column data was bilinearly interpolated at the latitude and

12   longitude of the aircraft flight path and was used to scale the standard TUV ozone profile (the

13   annual mean from the *U.S. Standard Atmosphere* [1976] for 45° N) to the measured value.

14   Absorption by SO_2 and NO_2 was not included in these model runs.

15   The OPAC Maritime Tropical aerosol profile from *Hess et al.* [1998] was used for the

16   majority of the TUV model runs discussed in this study. It has a total aerosol optical depth

17   (AOD) of 0.056 at 550 nm and a 2-km boundary layer. This Maritime Tropical boundary layer

18   has a single scattering albedo of 0.998 and an asymmetry parameter (g) of 0.774 (both at 550

19   nm) and represents a relatively clean background aerosol condition. For two of the case studies,

20   the OPAC Urban [*Hess et al.*, 1998] and *Elterman* [1968] aerosol profiles were employed (see

21   Table 1 for details). Unless otherwise stated the cloud-free sky TUV model (CFM) results refer

22   to calculations using the OPAC Maritime Tropical profile).

23   **2.3 Photolysis Frequency Calculation**

1   For each molecule of interest, the photolysis frequency is calculated from the actinic flux

2   spectrum, the absorption cross-section, and the quantum yield, which may vary as a function of

3   temperature and pressure. In this study, the most recent widely accepted molecular data were

4   used, and when possible the evaluations of *Sander et al*. [2000] were followed. The specific

5   details of the molecular parameters used in these calculations were recently reported in *Shetter et*

6   *al*. [2002]. The SAFS measured and TUV modeled actinic flux spectra were processed using the

7   same photolysis frequency calculation code to ensure that the same quantum yield, absorption

8   cross section, and temperature and pressure dependence relationships were applied to the

9   measured and modeled spectra.

10   Recently published results from the IPMMI show that Solar actinic flux can be measured

11   using a scanning spectroradiometers with spherical collection optics with an accuracy of about 5-

12   6% in the UV-A and about 6-7% at UV-B wavelengths [*Bias et al*., 2003; *Cantrell et al*., 2003].

13   Even without considering cloud/aerosol effects, it is difficult to assess the uncertainties in an

14   actinic flux derived from a radiative transfer model due to uncertainties in the extraterrestrial flux

15   and various model assumptions (e.g., vertical profiles of air, O_3, NO_2, SO_2). An intercomparison

16   of various radiative transfer models during IPMMI (including TUV) show that several radiative

17   transfer models could determine actinic flux to an accuracy of about 10% (as estimated from

18   comparison with observations and to the other model results) for clear-sky conditions with

19   relatively low aerosol loadings [*Bias et al*., 2003; *Cantrell et al*., 2003].

20   The overall accuracy of a measured or modeled photolysis frequency is heavily

21   influenced by the additional uncertainties in the available molecular data. These uncertainties

22   vary considerably from molecule to molecule, and are typically ± 5-10% for cross sections and

23   greater than ±10% for quantum yields. Therefore the error estimates are dominated by

1   uncertainties on the molecular data under cloud- and aerosol-free conditions. However, the

2   errors associated with the molecular data will not influence comparisons of the SAFS data with

3   radiative transfer model outputs since the identical cross section and quantum yield data are used

4   in the model and in the SAFS data reduction.

5   **2.4 LaRC 0-D Photochemical Box Model:**

6   The time-dependent photochemical box model used in these analyses has been described

7   previously [e.g., *Crawford et al.*, 1999b; *Olson et al.*, 2001]. The basic HO_X-NO_X-CH_4 gas-

8   phase chemistry is included with reactions and rates from *Atkinson et al.* [1992], *DeMore et al.*

9   [1997], and *Sander et al.,* [2000]. The nonmethane hydrocarbon (NMHC) chemistry is

10   calculated using the condensed mechanism of *Lurmann et al.* [1986] with modifications for

11   remote low-NO_X conditions to allow for the formation of organic peroxides. Additional changes

12   to the NMHC reactions include explicit chemistry for acetone, propane, and benzene. The wet

13   removal of soluble species is achieved using the mechanism of *Logan et al.* [1981]. These

14   particular model runs do not include any heterogeneous chemistry. A detailed list of the

15   reactions and rate coefficients used in this 0-D box model can be found in the appendix given by

16   *Crawford et al.*, [1999b]. Model calculations for instantaneous conditions were determined for

17   both the *in situ* measured (SAFS) and cloud-free sky TUV modeled (CFM) photolysis

18   frequencies.

19   Model input was derived from the official TRACE-P 1-minute averaged merged data set

20   (publicly available at http://www-gte.larc.nasa.gov). The information imbedded in the header of

21   the merged files describes the averaging procedures used in the creation of the merged data. The

22   model calculations were not performed unless observations of all of the following "critical"

23   photochemical parameters were available: O_3, CO, NO, dew/frost point temperature, and the

1   suite of photolysis frequencies. In addition, the model was only run for periods when the solar

2   zenith angle was less than 80 degrees. For NO measurements less than the 1-pptv limit-of-

3   detection, a NO value of 1 pptv was used for the calculation (208 points out of 8745 for the DC-8

4   data set and 213 points out of 9506 for P-3B data set). Some special consideration for NMHCs

5   was necessary to provide complete coverage for all model calculations as some 51% (DC-8) and

6   58% (P-3B) of NMHC measurements were concurrent with the 1-minute data merge. In most

7   cases (i.e., data gaps less than 5 minutes), NMHCs were simply averaged between consecutive

8   data grab samples. For data gaps larger than 5 minutes, only the nearest sample rather than an

9   average was used. In all, 98% of the calculations occur within a gap of 10 minutes or less

10   between grab samples.

11   Model runs using the SAFS photolysis rates were constrained to the measured NO, with

12   the NO_X partitioning determined by the measured photolysis frequencies. For the CFM model

13   runs, the box model was constrained to the same total NO_X as the SAFS case, but repartitioned

14   using the CFM calculated j-values. These particular model runs were not constrained by the

15   observed values of H_2O_2, CH_3OOH, HNO_3, and peroxyacetyl nitrate (PAN) to better illustrate

16   the potential differences between the model runs using the measured (SAFS) and modeled

17   (CFM) photolysis frequencies.

18   **3. Results**

19   During TRACE-P, 20 DC-8 flights (3 test + 17 transit/science flights) and 24 P-3B flights

20   (3 test + 21 transit/science flights) were flown. A summary of the major scientific results from

21   TRACE-P, as well as a brief description of each flight can be found in *Jacob et al.* [this issue].

22   A large variety of meteorological conditions were encountered during TRACE-P as the mission

23   spanned the transition from wintertime to springtime transport regimes. Consult *Fuelberg et al.*

1   [this issue] for a more complete report on meteorological conditions and transport pathways

2   encountered during TRACE-P. The photolysis frequency data from a few select flights

3   (presented below) was chosen as a clear example of either: a) sustained cloudy conditions (DC-8

4   Flight 15), b) cloud-free polluted conditions (DC-8 Flight 11 Profile 4), or c) cloud-free and

5   relatively pollution-free conditions (P-3B Flight17 Profile 2).

6   **3.1 Photolysis Frequency Measurement - Model Comparison**

7   An example of a period when clouds significantly impacted photolysis frequencies during

8   TRACE-P occurred while sampling convective outflow near a cold front to the south and west of

9   Japan on 27 March 2001 during DC-8 Flight 15 (Figure 1A). For much of this flight the

10   measured $j[NO_2{\rightarrow}NO+O(^3P)]$ (from now on referred to as jNO$_2$) is appreciably higher than the

11   CFM calculations (Figure 1A). For example there was a sustained period between 02:00-03:00

12   GMT, when there is a solid cloud deck below the aircraft and the measured total jNO$_2$ was 20-

13   80% higher than the total CFM values. On occasion, the instantaneous enhancement of jNO$_2$

14   due to clouds was larger than 200% (e.g, at 03:50 GMT during DC-8 Flight 15, Figure 1A).

15   Also note that the jNO$_2$ from the zenith viewing SAFS instrument during this flight showed very

16   close agreement with the jNO$_2$ determined from the downwelling components (direct beam and

17   downwelling diffuse) in the CFM (CFM$_{[dir+dwn]}$), while the SAFS nadir (or upwelling) jNO$_2$ was

18   often 1.5 to 3 times greater than the CFM determination (Figure 1A). In contrast, during the four

19   boundary layer sampling runs (at approximately 01:30, 03:30, 05:30, and 06:20 GMT) the DC-8

20   was below clouds and total SAFS jNO$_2$ was typically 45-90% less than the CFM.

21   Also on March 27th, the P-3B was investigating air-sea exchange and a volcanic plume

22   to the south and east of Japan in a relatively small, mostly cloud-free, region where subsident

23   conditions were prevalent (P-3B Flight 17). Much of this flight (from 01:45 – 04:00 GMT and

1   4:30 – 06:00 GMT) was flown in the boundary layer (i.e., below approximately 1200 m), and as

2   shown in Figure 1B, the measured $j[O_3 \rightarrow O_2 + O(^1D)]$, hereafter referred to as $jO(^1D)$, photolysis

3   frequencies were reduced by 30-40% compared to the CFM with Maritime Tropical aerosol

4   layer. Compared to $jO(^1D)$, the impact of aerosols in this boundary layer mixture of pollution

5   and volcanic SO_2 was slightly less for jNO_2, amounting to a reduction on the order of 15-20%, as

6   shown in a profile from 3.2 km to 0.23 km (Figure 2A). This implies a wavelength dependence

7   to the impact of aerosols on actinic radiation. However the comparison of measured and

8   modeled $jO(^1D)$ is always limited by how well the O_3 column is known. While model results by

9   *He and Carmichael* [1999] show a similar response for both $jO(^1D)$ and jNO_2 to aerosols at local

10   noon, a sensitivity analysis by *Reuder and Schwander* [1999] indicates that aerosols will impact

11   $jO(^1D)$ more than jNO_2 at a solar zenith angle (SZA) of 40º and less than jNO_2 at a SZA of 70º.

12   *Dickerson et al.* [1997] suggest that the wavelength and SZA dependence of the aerosol impact is

13   related to the changes in the direct-to-diffuse ratio, since more of the direct solar beam is

14   converted to diffuse radiation at shorter wavelengths, at larger SZA, and at thicker aerosol

15   optical depths. During the P-3B profile in Figure 2A, the SAFS and CFM upwelling jNO_2 are

16   quite similar, so that almost all of the absolute reduction appears to be in the downwelling

17   (diffuse and direct beam) components of the UV-A radiation that constitute jNO_2. In a relative

18   sense, the upwelling discrepancies are not substantially different from the downwelling ones,

19   especially above 2 km.

20   Given that the OPAC Maritime Tropical aerosol profile represents a fairly low aerosol

21   optical depth (τ) of 0.056, CFM calculations with higher total aerosol loadings of 0.380

22   (Elterman Profile) and 0.643 (OPAC Urban Profile) were also performed for this same case

23   during P-3B Flight 17 (Figure 2B). In this application, the Elterman profile has a constant single

1   scattering albedo (ω) of 0.99 or 0.85, a constant asymmetry parameter (g) of 0.60, and a constant

2   Angstrom Coefficient (α) of 1.00 for all layers of the model. The OPAC aerosol profiles have

3   different aerosol optical properties for the boundary layer, free troposphere, and stratosphere

4   sections of the model. Please refer to Table 1 for specific information regarding the optical

5   properties of the different aerosol profiles used in this study.

6   The Elterman profile with a highly scattering aerosol (ω of 0.99) resulted in the highest

7   CFM $j\mathrm{NO_2}$ throughout the atmospheric column, but gave a similar result to the Maritime

8   Tropical CFM $j\mathrm{NO_2}$ at the bottom of the sampling profile. The CFM with more-absorbing

9   aerosol profiles (Urban and Elterman with ω of 0.85) have significantly lower values for $j\mathrm{NO_2}$ at

10   the lowest measurement altitude compared to the CFM Maritime Tropical case (Figure 2B). The

11   CFM with the Urban profile resulted in an underestimate of the SAFS $j\mathrm{NO_2}$ in the bottom 750

12   meters of the atmosphere. It is readily apparent that the CFM with all of these "standard" aerosol

13   profiles does not agree with the conditions encountered between 2 km and 3 km during this

14   aircraft spiral, as shown by the poor agreement (none better than 15%) with the total SAFS $j\mathrm{NO_2}$

15   (Figure 2B). The CFM was also run without any aerosols and the results were quite similar to

16   the Maritime Tropical case (not shown).

17   During TRACE-P the DC-8 aircraft attempted some aircraft profiles in cloud-free areas

18   to provide data to help calibrate the MOPITT satellite, and as a consequence a number of spirals

19   were collected in relatively cloud-free regions over the Pacific Ocean. During the MOPITT

20   spiral on DC-8 flight 11, the use of the Maritime Tropical aerosol profile in CFM resulted in a

21   modeled $j\mathrm{NO_2}$ profile that was approximately 9% greater than the SAFS measurements (Figure

22   3A). The CFM $j\mathrm{O}(^1\mathrm{D})$ showed much better agreement during this cloud free spiral with the

23   SAFS-to-CFM disagreement ranging from -1 to $+6$% (Figure 3B). Running the CFM with

1   different aerosol profiles for this MOPITT spiral did not significantly improve the agreement

2   with the jNO$_2$ SAFS measurements (Figure 3C), however using the more-absorbing Elterman

3   profile (ω of 0.85) did give a similar jNO$_2$ for the lowest measurement altitude (168 m). More

4   information regarding the geographic parameters of these case study profiles can be found in

5   Table 2. Detailed information about the TRACE-P campaign as well as the entire merged

6   TRACE-P dataset is publicly available at http://www-gte.larc.nasa.gov.

7   **3.2 Cloud Impact Factor**

8   A more quantitative way of addressing the SAFS and CFM agreement is to examine the

9   SAFS-to-CFM ratio, also known as the J-Value Impact Factor (JIF). As shown in the previous

10   results, the JIF is slightly different for the photolysis frequencies of different molecules, but our

11   analysis has shown that the different JIFs are highly correlated with each other as expected (i.e.,

12   when jNO$_2$ is reduced or enhanced by a cloud, so is jO(^{1}D)). Ideally, a JIF of 1.0 would occur

13   during cloud-free conditions, thus representing perfect agreement between SAFS and the CFM.

14   For this campaign, the SAFS / CFM agreement is generally observed at a JIF between 0.80 and

15   1.00. The use of incorrect aerosol optical properties in the CFM is the most likely reason for this

16   offset. Since the JIFs discussed in this study were calculated with a CFM using the OPAC

17   Maritime Tropical profile (which has an extremely light aerosol loading), the influence of

18   pollution aerosols on the reported JIFs should be visible if they are significant. As clouds can

19   have significantly higher optical depths compared to aerosol layers, they would seem to be

20   responsible for the larger changes in JIF. Because clouds impact the UV-A and visible portions

21   of the spectrum more than the UV-B [*Seckmeyer et al.*, 1996; *Crawford et al.*, 2002], then the

22   jNO$_2$ JIF should be a more sensitive indicator of cloud influences than the jO(^{1}D) JIF.

1   In Figure 4A the jNO$_2$ JIF is shown for all of TRACE-P (for both the DC-8 and P-3B

2   aircraft) as a function of altitude. For both aircraft there is a large cluster of points between 0.80

3   and 1.0 at all altitudes. In general, the JIFs less than 0.85 occur at altitudes below 1 km, and the

4   JIFs greater than 1.0 are found above 2 km (Figure 4A). Overall, the jNO$_2$ JIFs are normally

5   distributed but exhibit a slight skewness towards values greater than 0.95 (Figure 4B). When the

6   JIF distribution is separated into three altitude populations (0-1 km, 1-5 km, and 5-12 km (Figure

7   4B)), it reveals that reduced radiation environments were much more common below 1 km and

8   that enhanced radiation was more prevalent above 1 km.

9   The peaks of these different altitude populations occur at slightly different JIF values,

10   with the JIFs below 1 km showing a majority of the values between 0.80 and 0.95, while the

11   peaks for the higher altitude groups maximizing between 0.85 and 1.00 values of JIF. The

12   significance of the different locations for the peaks suggests that the CFM with Maritime

13   Tropical aerosol profile does not perform as well below 1 km as above 1 km. This is not

14   surprising given that the bulk of the aerosol loading is typically in the bottom 1 km of the

15   atmosphere.

16   Considering that the SAFS to CFM comparisons shown in the two cloud-free spirals (one

17   in a polluted environment (Figure 2) and one in a relatively clean atmosphere (Figure 3)) give

18   JIFs in the range of 0.85 to 0.95, one could make the argument that these jNO$_2$ JIF values

19   represent periods when the aircraft was in cloud-free skies. This assumption is based on the idea

20   that the majority of the time above 1 km the aircraft was in a cloud-free environment, with

21   significant changes in the radiation environment resulting from the influence of clouds. This

22   idea is also represented graphically in Figure 4A which shows a heavy concentration of points

23   between 0.80 and 1.00 at all altitudes. Similarly, a complementary analysis by *Tang et al*. [this

issue] indicates that the general aerosol impact on j-values during TRACE-P was to reduce the

photolysis frequencies uniformly throughout the atmospheric column. This would mean that

away from the influence of clouds, one would expect a CFM with a clean aerosol profile to

overestimate the SAFS measurements.

Given the assumption that a JIF of 0.80-1.00 represents cloud-free conditions, it is

possible to calculate that overall, 40% of the TRACE-P dataset was collected in cloud-free sky

conditions, 45% in a enhanced radiation environment, and 15% in a reduced radiation

environment (Figure 4B, inset). As shown in Figure 4B, 80% of the combined dataset was

collected at altitudes above 1 km, where enhancements due to clouds below the aircraft were

much more common than reductions due to clouds above the aircraft. Below 1 km reduced jNO$_2$

values were much more common compared to enhanced photolysis. In fact JIFs less than 0.80,

corresponding to a jNO$_2$ significantly reduced by clouds and/or aerosols, represent the most

common situation below 1 km during TRACE-P (Figure 4B, inset).

4.0 Discussion

4.1 How well do photolysis frequencies modeled with "standard" aerosol profiles agree

with the measurements?

4.1.1 Cloudy Atmospheres. The JIF analysis suggests that the DC-8 and P-3B aircraft

only encounter "cloud-free" skies 40% of the TRACE-P campaign, thus it is relatively common

to have a flight were the cloud-free assumption does not hold. A graphic example of the cloud

effect on photolysis frequencies occurred during DC-8 flight 15 when the SAFS j-values did not

agree to within 50% of the CFM for most of the flight (Figure 1A). Clouds appear to have a

large impact on UV radiation and it is likely that the frequent occurrence of clouds during the

TRACE-P experiment would also apply to other locations in the mid-latitudes.

1   One simple approach to incorporating clouds into modeling airborne photolysis

2 frequency measurements is to use a satellite albedo measurement to determine if there are clouds

3 present in the measurement region. *Shetter et al.* [2002] showed that using the TOMS albedo as

4 input into a radiative transfer model did substantially improve their aircraft measurement-model

5 photolysis frequency agreement when the aircraft was above a solid deck of clouds. However,

6 the TOMS albedo method significantly degraded the SAFS to CFM agreement for periods when

7 the aircraft was below the cloud layer. In addition, the TOMS pixel size (1° latitude x 1.25°

8 longitude) is large relative to the volume of the atmosphere impacting the aircraft actinic flux

9 measurements, so while the aircraft may be in a clear patch near some clouds, the TOMS satellite

10 may indicate a cloudy pixel. Since there was no way to know the cloud top heights or the cloud

11 thickness from satellite albedo data, a potential improvement of this approach might be to use IR

12 satellite products that can estimate cloud top heights. This will still not solve the problem of

13 broken and scattered clouds or multiple cloud layers that are common in tropical and temperate

14 regions but may also be a tool to estimate cloud thickness.

15   A different method for dealing with clouds is to use a regional meteorological model to

16 determine the cloud fields in three dimensions. In Part II of this TRACE-P study, *Tang et al.*

17 [this issue] have coupled the STEM (v. 2K1) 3-D regional scale chemical transport model

18 (CTM) to a version of the TUV radiative transfer model. From this large-scale model it is

19 possible to extract the vertical profile of clouds and aerosol optical properties and then run the

20 radiative transfer calculations for the extracted profile. Since this CTM did a fairly good job of

21 modeling the cloud presence and dimensions for significant cloud formations, it is encouraging

22 that STEM/TUV calculation captures enhancements above clouds and reductions below clouds

23 during DC-8 Flight 15 (see Figure 11 of *Tang et al.*, [this issue] for more details).

1   **4.1.2 Clear Atmosphere.** Even during the cloud-free conditions there are no guarantees

2   that the standard CFM is going to agree with the measurements as aerosols also impart a notable

3   impact on radiative transfer. During P-3B flight 17 to a significantly polluted but relatively

4   cloud-free region of the Pacific Ocean, the CFM calculations of jNO$_2$ were commonly 20%

5   higher than the SAFS (Figures 1B and 2A). For this specific jNO$_2$ profile the CFM was also run

6   with some polluted aerosol profiles, but the agreement with the SAFS jNO$_2$ was not much better.

7   It appears that the aerosols encountered in this region on this day were significantly more

8   absorbing than any of the "standard" profiles employed by the model. The fact that none of the

9   CFM simulations gets close to the measured jNO$_2$ at the top of the profile suggests that the free

10   troposphere above this location also contained significant absorbing aerosol. This decrease is

11   more than the 6-11% decreases in tropospheric photolysis frequencies that *Liao et al.* [1999]

12   found for soot aerosol, but closer to the 20-30% decreases observed by *Papayannis et al.* [1998]

13   for a polluted site in Greece.

14   On the other hand, it is heartening that the CFM agreement with the SAFS jNO$_2$ and

15   jO(^{1}D) is much better during the cloud-free DC-8 MOPITT validation profile during flight 11

16   (Figures 3A and 3B). At this relatively remote (i.e., clean) location, the CFM with the Maritime

17   Tropical aerosol profile resulted in SAFS agreement better than 9% for jNO2 and better than 5%

18   for jO(^{1}D). It is often difficult to evaluate jO(^{1}D) model agreement since this photolysis

19   frequency is so sensitive to having the correct overhead ozone column as a model input;

20   nevertheless, it is encouraging that the CFM and SAFS jO(^{1}D) values are so close. Using the

21   CFM with additional polluted profiles did improve the jNO$_2$ SAFS-to-CFM agreement at the

22   bottom of the aircraft spiral, but did not improve the disagreement at 10 km. This is difficult to

23   understand as the previous measurements at high altitude during the SOLVE campaign show

1   significantly better agreement between the SAFS and CFM (with Elterman aerosol profile) at

2   high altitudes. Indeed, there is a slight slope to the altitude distribution of the jNO$_2$ JIF (Figure

3   4A) with "cloud-free" JIF values closer to 0.95 occurring at the top altitudes (12 km) compared

4   to JIFs of approximately 0.85 in the boundary layer.

5   Overall, for the combined DC-8 and P-3 dataset, the mean jNO$_2$ JIF is 0.943± 0.271

6   (0.929 median) and for jO(^{1}D) the mean and median SAFS to CFM ratios are 0.932± 0.270 and

7   0.937, respectively. Compared to the PEM-Tropics B mission, the TRACE-P SAFS to CFM

8   ratios are similar for jO(^{1}D), but slightly higher than the jNO$_2$ measurement/model ratios

9   reported by *Shetter et al*. [2002]. The primary difference between the these two missions was the

10   use of the Elterman aerosol profile ($\omega = 0.99$) for the PEM-Tropics B CFM, while the OPAC

11   Maritime Tropical profile was employed in this study as the "background" aerosol, which could

12   account for some of the differences in the average measurement / model ratios.

13   Previous studies have suggested that even in idealized cloud-free conditions, spectrally

14   resolved UV radiative transfer models need well-specified aerosol input parameters to get results

15   within ±10% of the measurements. [*Weihs and Webb*, 1997b; *Papayannis et al*., [1998]. In a

16   study by *Reuder and Schwander* [1999], it was shown that τ and ω are the two key factors to

17   describe the radiative effects of aerosols, together describing more than 80% of the change in the

18   UV transmission due to aerosols. According to *Weihs and Webb* [1997a], uncertainties in

19   radiative transfer models can be attributed to the uncertainty in: (a) the extraterrestrial flux used

20   by the model (TUV uses a hybrid SUSIM-Atlas3-Neckel & Labs extraterrestrial flux spectra

21   [*van Hoosier et al*., 1987; *Neckel and Labs*, 1984]), (b) the uncertainty in inputs of aerosol

22   optical parameters such as ω, g, and τ; (c) the uncertainty in albedo input, and (d) the uncertainty

23   in overhead ozone column input (for UV-B wavelengths only). Depending on the conditions, the

1   propagation of these different uncertainties limit the absolute accuracy of a typical CFM

2   calculation to between ±19% to ±26% for UV-B wavelengths and ±5% to ±15% for the UV-A

3   wavelengths [*Weihs and Webb*, 1997a]. The comparison presented in Figure 3 reveals that the

4   SAFS is about 9% lower than the CFM (with OPAC Maritime Tropical Profile) for cloud-free

5   low-aerosol conditions. While this is not perfect agreement, considering the uncertainties in the

6   model and the measurements, this is the order of the agreement one can expect for a radiative

7   transfer model without having better defined aerosol optical properties.

8   **4.2 Photochemical Implications**

9   **4.2.1 Photochemical box model sensitivity to photolysis frequency inputs.** Radiative

10   transfer models will never be able to calculate photolysis frequencies with absolute accuracy.

11   Much of the time, primarily due to the lack of sufficient input data, model j-values may be in

12   error by a considerable amount. This brings up the question of how accurate photolysis

13   frequency calculations need to be to give "realistic" results from a photochemical box model.

14   To analyze the impact of changes in the UV radiation environment on photochemistry,

15   the LaRC 0-D photochemical box model was run for the DC-8 and P-3B TRACE-P data merge,

16   once with the SAFS- and a second time with the CFM-calculated suite of photolysis frequencies.

17   An example of the impact of clouds on photochemistry is shown in Figure 5A where the steady-

18   state [OH] concentration increases as the UV radiation is enhanced. In this figure, the ratio of the

19   [OH] calculated with the SAFS j-values ([OH]$_{SAFS}$) over the [OH] calculated from the CFM

20   photolysis frequencies ([OH]$_{CFM}$) is plotted as a function of the $jO(^1D)$ JIF. OH, as well as HO$_2$

21   and H$_2$O$_2$ have been plotted versus the $j(O^1D)$ JIF since it more closely governs their abundance.

22   Other species have been plotted versus the $j(NO_2)$ JIF.

1   The color of the symbols on Figure 5 is an indicator of the altitude of the aircraft at the

2   time of the measurement with the red indicating the boundary layer (0 to 1 km), green the lower

3   troposphere (1 to 5 km), and blue the upper free troposphere (5 to 12 km) samples. As was

4   shown in Figure 4B, most of the JIF values less than 0.8 are the red (lower altitude) points and

5   the JIF symbols for values greater than 1.0 are mostly blue and green (higher altitudes).

6   From Figure 5A, the steady-state OH concentration has a linear relationship to changes in

7   jO(^{1}D) with a slope less than unity (slope = 0.894, intercept = 0.072). This suggests that the

8   direct production of OH from O(^{1}D) and H_2O was the dominant source of OH during TRACE-P,

9   while the primary OH sinks (i.e., OH + CO, OH + CH_4) did not vary with changes in photolysis

10   frequencies. Consequently, if the modeled j-values were incorrectly 50% high (e.g., a JIF of 0.5

11   due to the aircraft being under a cloud), the calculated [OH] would also be almost 50% higher

12   than if the correct photolysis frequencies were used.

13   Most other species have a less direct relationship. The [HO$_2$]$_{SAFS}$ to [HO$_2$]$_{CFM}$ ratio

14   increases with increasing UV radiation (Figure 5B), but in this case it is best described by a

15   power function with almost a square root dependence of 0.526 (i.e., [HO$_2$]$_{SAFS}$ / [HO$_2$]$_{CFM}$ =

16   0.991 [jO(^{1}D)JIF] $^{0.526}$). In a low-NO$_X$ environment, a linear increase in HO$_2$ production is

17   counteracted by a quadratic increase in HO$_2$ loss through the HO$_2$ + HO$_2$ self-reaction (i.e.,

18   2·α·jO(^{1}D) = k[HO$_2$][HO$_2$], where α is the fraction of O(^{1}D) reacting with H_2O). Thus, it is not

19   surprising that changes in the steady-state HO$_2$ concentration in response to variations in the j-

20   values has a square root dependence (i.e., [HO$_2$] = (2·α·jO(^{1}D)/k)$^{0.5}$). Accordingly, if the CFM

21   values were 40% lower than true photolysis frequencies (e.g., JIF of 1.67 due to cloud below

22   aircraft), the incorrectly calculated [HO$_2$] would be approximately 23% low. Notice that in

23   Figure 5B, a handful of blue data points at JIF values of 1.1-1.2 lie significantly above the rest of

1   the data. These points are associated with the highest upper tropospheric NO values observed

2   during TRACE-P (600-800 pptv) as compared to the median value of just under 20 pptv. As

3   noted earlier, radical-radical losses of HO_x dominate only in a low NO_x environment. For these

4   data points, HO_2 loss is dominated by conversion of HO_2 to OH via HO_2+NO followed by

5   formation of HNO_3 via $OH+NO_2$. Thus, the loss of HO_2 is linear rather than quadratic, allowing

6   for larger increases in HO_2 for a given increase in $j(O^1D)$. Recognize that these conditions

7   represent the exception rather than the rule for the TRACE-P data.

8   Behavior similar to that of HO_2 is observed for H_2O_2 (see Figure 5C) and CH_3O_2 (not

9   shown). H_2O_2 is directly related to HO_2 in that it is produced through the HO_2+HO_2 reaction.

10 CH_3O_2 (not shown) behaves similarly to HO_2 in that its loss is regulated through self reaction as

11 well as reaction with HO_2 ($[CH_3O_2]_{SAFS}/[CH_3O_2]_{CFM} = 0.993(jO(^1D)$ JIF$)^{0.414}$, $r^2 = 0.937$).

12 Trends in NO and NO_2 with changes in UV radiation are shown in Figures 5D and 5E

13 respectively. Since the absolute level of NO_x ($NO+NO_2$) does not change between the SAFS and

14 CFM calculations, these trends reflect changes in NO_x partitioning with changes in UV. There

15 are no surprises in that NO_2 decreases with increasing $j(NO_2)$ JIF while NO increases. There is,

16 however, some interesting behavior in that the responses vary with altitude. For NO, low

17 altitude data (red points) experience the greatest change, whereas relatively small changes occur

18 at high altitude (blue points). The response of NO_2 is the opposite, with the largest changes at

19 high altitude and smallest changes near the surface. This behavior can be explained by the

20 change in the NO_x partition with altitude (see Figure 6).

21   The partitioning of NO_x is largely determined by the competition between NO_2 photolysis

22 and reaction of NO with O_3. In the lower atmosphere, NO_2 photolysis tends to be slower than

23 $NO+O_3$ allowing for NO_2 to be the dominant species. While NO_2 photolysis increases modestly

1   with altitude, the kinetic rate coefficient for $NO+O_3$ decreases by a factor of 5 between the

2   surface and 12 km, thus leading to a shift in favor of NO as the dominant species in the upper

3   troposphere. Since changes in UV radiation lead to changes in the NO_x partitioning, the lesser

4   species always experiences the larger absolute change (i.e., NO in the lower troposphere and

5   NO_2 in the upper troposphere).

6   When photolysis frequencies decreased in the atmosphere, the steady-state HCHO

7   concentrations decrease as well (Figure 5F). This effect appears to be the strongest in the

8   boundary layer and considerably weaker in the upper troposphere. HCHO is derived

9   predominantly from the CH_3O_2+NO reaction and lost via photolysis and reaction with OH.

10   Under reduced UV, which tends to occur in the lower troposphere, the reduction in HCHO

11   production is roughly quadratic since both CH_3O_2 and NO are decreased while the decrease in

12   HCHO loss via photolysis and OH is roughly linear. This leads to an overall reduction in

13   HCHO. By contrast, for increased UV conditions in the upper troposphere, relative changes in

14   HCHO sources and sinks appear to be roughly balanced. This is most likely related to the

15   reduced sensitivity of NO in the upper troposphere (see Figure 5D), weakening the potential

16   quadratic effect of the CH_3O_2+NO source.

17   PAN (Figure 5G) appears to have three fundamentally different responses to changes in

18   UV radiation, one at lower altitudes (red points), one at higher altitudes (blue points), and an

19   intermediate response in the lower troposphere (green points). These responses are best

20   understood by examining the trends in its precursors, NO_2 and $CH_3C(O)O_2$, both of which have

21   opposite responses to changes in UV intensity. The peroxy acetyl radical ($CH_3C(O)O_2$) (Figure

22   5H) shows a relationship with changes in the JIF similar to HO_2 and NO_2, with $[CH_3C(O)O_2]$

23   increasing with increasing UV radiation to the power of 0.510. In the lower troposphere (red

1   points), where changes in NO_2 are weakest, the trend for PAN closely mirrors that of

2    $CH_3C(O)O_2$. In the upper troposphere (blue points), where NO_2 exhibits the greatest sensitivity,

3   PAN mimics the response of NO_2. These competing factors appear to balance in the middle

4   troposphere with PAN showing little response to changes in UV.

5   For the TRACE-P chemical environment, a few species, such as OH, NO, and HO_2, were

6   quite sensitive to changes (or errors) in photolysis frequencies, while $CH_3C(O)O_2$, CH_3OOH,

7    $HONO_2$, HO_2NO_2, and other aldehydes were less sensitive. A third group of compounds,

8   including NO_2, PAN, and HCHO, exhibited one photochemical relationship in the boundary

9   layer and a different response in the free troposphere. Consequently, it seems that the desired

10   accuracy of a photolysis frequency value depends on what question you are asking. If you are

11   interested in calculating the steady-state [OH] within 10%, then you need to measure or model

12   the real world j-values with a similar accuracy. In contrast, the steady-state $HONO_2$

13   concentration is not as strongly impacted by errors in photolysis frequency determination.

14   **4.2.2 Ozone production and loss.** Changes in the ozone production rate (P_{O3}) have a

15   strong relationship to changes in $j$$NO_2$, with a linear slope of 0.985 (Figure 7A). Consequently, a

16   10% error in the CFM j-value calculation will result in about a 10% error in the modeled O_3

17   production rate. Similarly, increases in the actinic flux will also linearly increase the rate of

18   chemical O_3 destruction (Figure 7B). It is important to note that the slope of the O_3 chemical

19   loss rate is 20% less than the slope of the O_3 production rate. Thus while an enhancement in the

20   UV environment above a cloud may increase both the O_3 loss and production rates, it appears to

21   increase the production rate slightly more, leading to a net increase in the O_3 tendency (Figure

22   7C). The ratio plot of the O_3 tendency versus JIF is quite scattered; this is a result of the fact that

23   the O_3 tendency is the difference between the O_3 production and loss rates. At higher JIF values,

1   this is the ratio of the difference of two large numbers; thus the result can be large or small and

2   positive or negative. Overall, the outliers cancel each other out and the central trend is for a

3   linear increase (slope = 0.947±0.032, y-intercept = 0.008±0.031) in the O_3 tendency with

4   increased UV radiation.

5   During the TRACE-P campaign approximately 20% of these samples were collected at

6   altitudes less than 1 km. More than half of that time the DC-8 and P-3 were experiencing a

7   reduced UV actinic flux in or just above the marine boundary layer (Figure 4B). The attenuated

8   solar flux encountered in the 0-1 km range, where O_3 production is usually higher than O_3

9   destruction, resulted in a 60% reduction in the net O_3 tendency, as compared to box model

10   calculations using the CFM *j*-values (Figure 8). Previous studies have also predicted a reduction

11   in surface O_3 due to absorbing aerosols (e.g., *He and Carmichael*, 1999; *Jacobson*, 1998], while

12   other studies have seen an increase in boundary layer O_3 mixing ratios due to scattering aerosols

13   [e.g., *Dickerson et al.*, 1997]. The reduced boundary layer O_3 tendencies observed during

14   TRACE-P (as compared to a CFM model with standard aerosol profiles) is consistent with this

15   being an attenuated UV radiation environment due to absorbing pollution aerosols and cloudy

16   conditions. The remaining 80% of the mission flight hours were spent sampling in the free

17   troposphere. In the lower troposphere during TRACE-P, the overall photochemical tendency

18   was weak, with similar production and loss rates. In this environment, the net effect of clouds

19   and aerosols was a modest (1-6%) decrease in both loss rates, resulting in an insignificant change

20   on the net O_3 tendency at altitudes from 1 to 5 km (Figure 8). In contrast, the upper tropospheric

21   photochemical environment favored net ozone production, where the net impact of the cloud

22   enhanced UV conditions was a modest increase (on the order of 9%) in the net O_3 tendency for

23   the 5-12 km altitude region.

1   **5.0 Conclusions**

2   The objective of this study was to analyze the agreement between the measured and

3   modeled (using standard aerosol profiles) atmospheric photolysis frequencies during the

4   TRACE-P mission and to investigate the significance of changes in the UV environment on

5   ozone photochemistry as determined by a 0-D photochemical box model. The jNO$_2$ observed

6   mean and median JIF ratios between approximately 15,800 1-minute averaged measured SAFS

7   and CFM calculated j-values were 0.943±0.271 and 0.929, respectfully. The variability in this

8   measurement to model ratio was a result of the impact of clouds and aerosols on UV radiative

9   transfer. Considering that the TRACE-P atmosphere was "cloud-free" 40% of the time, a model

10   with a cloud-free assumption is only going to be valid part of the time.

11   During TRACE-P it appears that clouds had a larger instantaneous impact on photolysis

12   frequencies (ranging from –90 to +200%) than aerosols (maximum of -20%) as compared to a

13   CFM with a "standard" aerosol profile. Even in an ideal (cloud-free and low-AOD) atmosphere,

14   the CFM and SAFS j-values differed by some 9% for jNO$_2$. However, the agreement during

15   these conditions was much better for jO(^{1}D) (-2 to +7%). These results and RT model

16   uncertainty analysis from previous studies [e.g., *Weihs and Webb*, 1997a,b; *Papayannis et al.*,

17   1998; *Reuder and Schwander*, 1999] suggest that it may be difficult to get measurement/model

18   agreement to better than 10% without have better knowledge of the key aerosol optical properties

19   such as aerosol optical depth and single scattering albedo, even for cloud-free conditions.

20   Modeled j-values will not be accurate much of the time in a complex atmosphere, which

21   makes it reasonable to ask how accurate photolysis frequency calculations need to be as inputs to

22   a photochemical box model. For the TRACE-P chemical environment, a few species, such as

23   OH, NO, and HO$_2$, were more sensitive, while other compounds (e.g. CH$_3$C(O)O$_2$, CH$_3$OOH,

1   HONO$_2$, HO$_2$NO$_2$, and other aldehydes) were less sensitive to changes (or errors) in the suite of

2   photolysis frequencies. A third group of compounds such as NO$_2$, PAN, and HCHO, exhibited

3   one photochemical relationship in the boundary layer and a different response to UV radiation in

4   the free troposphere. PAN displayed the most divergent behavior between the three altitude

5   groups, which relates to the different responses in its precursors. The O$_3$ production and loss

6   rates linearly increase and decrease with changes (or errors) in the photolysis frequency inputs,

7   with the production changing with a steeper slope than the O$_3$ loss rate. The net O$_3$ tendency has

8   a positive linear response (with a slope close to 1) to changes in photolysis frequencies; thus a

9   10% enhancement (or underestimate error) in the j-values due to clouds or aerosols would result

10   in approximately a 10% increase (or underestimate error) of the instantaneous net O$_3$ tendency.

11   The net photochemical effect of clouds and aerosols during the TRACE-P campaign was a large

12   decrease photochemical O$_3$ production in the boundary layer.

13

9 **References**

10 Atkinson, R., D.L. Baulch, R.A. Cox, R.F. Hampson, J.A. Kerr, and J. Troe, Evaluated kinetic and photochemical

11   data for atmospheric chemistry, Supplement IV, IUPAC subcommittee on gas kinetic data evaluation for

12   atmospheric chemistry, *J. Phys. Chem. Ref. Data*, *21*, 1125-1568, 1992.

13 Balis, D.S., C.S. Zerefos, K. Kourtidis, A.F. Bais, A. Hofzumahaus, A. Kraus, R. Schmitt, M. Blumthaler, and G.P.

14   Gobbi, Measurements and modeling of photolysis rates during the Photochemical Activity and Ultraviolet

15   Radiaiton (PAUR) II campaign, *Journal of Geophysical Research*, *107* (D18), 8138,

16   doi:1029/2000JD000136, 2002.

17 Castro, T., S. Madronich, S. Rivale, A. Muhlia, and B. Mar, The influence of aerosols on photochemical smog in

18   Mexico City, *Atmospheric Environment*, *35* (10), 1765-1772, 2001.

19 Crawford, J., D. Davis, G. Chen, R. Shetter, M. Müller, J. Barrick, and J. Olson, An assessment of cloud effects on

20   photolysis rate coefficients: Comparison of experimental and theoretical values, *J. Geophys. Res.*, *104*

21   (D5), 5725-5734, 1999a.

22 Crawford, J*., et al.*, Assessment of upper tropospheric HOx sources over the tropical Pacific based on NASA

23   GTE/PEM data: Net effect on HOx and other photochemical parameters, *J. Geophys. Res.*, *104* (D13),

24   16,255-16,274, 1999b.

25 Crawford, J., R. Shetter, B. Lefer, C. Cantrell, W. Junkerman, S. Madronich, and J. Calvert, Cloud impacts on UV

26   spectral actinic flux observed during IPMMI, *Journal of Geophysical Research*, *submitted*, 2002.

1 DeMore, W.B., M.J. Molina, S.P. Sander, D.M. Goldan, C.E. Kolb, R.F. Hampson, M.J. Kurylo, C.J. Howard, and
2   A.R. Ravishankara, Chemical kinetics and photochemical data for use in stratospheric modeling, *JPL Publ.,*
3   *97-4*, 1997.

4 Dickerson, R.R., S. Kondragunta, G. Stenchikov, K.L. Civerolo, B.G. Doddridge, and B. N.Holben, The impact of
5   aerosols on solar ultraviolet radiation and photochemical smog, *Science*, *278*, 827-830, 1997.

6 Elterman, L., UV, visible, and IR attenuation for altitudes to 50 km, *Rep. AFCRL-68-0153*, Air Force Cambridge
7   Res. Lab., Cambridge, Mass., 1968.

8 Feister, U., and R. Grewe, Spectral Albedo Measurements in the UV and Visible Region over Different Types of
9   Surfaces, *Photochemistry and Photobiology*, 62 (4), 736-744, 1995.

10 Fuelberg, H.E., C.M. Kiley, J.R. Hannan, D.J. Westberg, M.A. Avery, and R.E. Newell, Meteorological conditions
11   and transport pathways during the Transport and Chemical Evolution over the Pacific (TRACE-P)
12   experiment, *Journal of Geophysical Research*, this issue, 2003.

13 Früh, B., T. Trautmann, M. Wendisch, and A. Keil, Comparison of observed and simulated NO_2 photodissociation
14   frequencies in a cloudless atmosphere and in continental boundary layer clouds, *Journal of Geophysical*
15   *Research-Atmospheres*, *105* (D8), 9843-9857, 2000.

16 He, S., and G.R. Carmichael, Sensitivity of photolysis rates and ozone production in the troposphere to aerosol
17   properties, *Journal of Geophysical Research-Atmospheres*, *104* (D21), 26307-26324, 1999.

18 Hess, M., P. Koepke, and I. Schult, Optical properties of aerosols and clouds: The software package OPAC, *Bulletin*
19   *of the American Meteorological Society*, *79* (5), 831-844, 1998.

20 Hofzumahaus, A., A. Kraus, A. Kylling, and C.S. Zerefos, Solar actinic radiation (280-420 nm) n the cloud-free
21   troposphere between ground and 12 km altitude: Measurements and model results, *Journal of Geophysical*
22   *Research*, *108* (D18), 8139, doi:10.1029/2001JD900142, 2002.

23 Jacob, D.J., J.H. Crawford, M.M. Kleb, V.E. Connors, R.J. Bendura, J.L. Raper, G.W. Sachse, J.C. Gille, and L.
24   Emmons, The Transport and Chemical Evolution over the Pacific (TRACE-P) Mission: Design, execution,
25   and first results, *Journal of Geophysical Research-Atmospheres*, this issue, 2003.

26 Jacobson, M.Z., Studying the effects of aerosols on vertical photolysis rate coefficient and temperature profiles over
27   an urban airshed, *Journal of Geophysical Research-Atmospheres*, *103* (D9), 10593-10604, 1998.

1　Junkermann, W*., et al.*, Actinic radiation and photolysis processes in the lower troposphere: Effect of clouds and

2　　aerosols, *Journal of Atmospheric Chemistry*, *42* (1), 413-441, 2002.

3　Lantz, K.O., R.E. Shetter, C.A. Cantrell, S.J. Flocke, J.G. Calvert, and S. Madronich, Theoretical, actinometric, and

4　　radiometric determinations of the photolysis rate coefficient of NO2 during the Mauna Loa observatory

5　　photochemistry experiment 2, *Journal of Geophysical Research-Atmospheres*, *101* (D9), 14613-14629,

6　　1996.

7　Lefer, B.L., S.R. Hall, L. Cinquini, J.D. Barrick, J.H. Crawford, and R.E. Shetter, Comparison of airborne NO_2

8　　photolysis frequency measurements during PEM-Tropics B, *Journal of Geophysical Research*, *106* (D23),

9　　32,645-32,656, 2001.

10　Liao, H., Y.L. Yung, and J.H. Seinfeld, Effects of aerosols on tropospheric photolysis rates in clear and cloudy

11　　atmospheres, *J. Geophys. Res.*, *104* (D19), 23,697-23,708, 1999.

12　Liu, S.C., S.A. McKeen, and S. Madronich, Effect of anthropogenic aerosols on biologically active ultraviolet

13　　radiation, *Geophys. Res. Lett.*, *18* (12), 2265-2268, 1991.

14　Logan, J.A., M.J. Prather, S.C. Wofsy, and M.B. McElroy, Tropospheric Chemistry: a global perspective, *Journal*

15　　*of Geophysical Research*, *86* (C8), 7210-7254, 1981.

16　Lurmann, F.W., A.C. Lloyd, and R. Atkinson, A Chemical Mechanism for Use in Long-Range Transport Acid

17　　Deposition Computer Modeling, *Journal of Geophysical Research-Atmospheres*, *91* (D10), 905-936, 1986.

18　Ma, J.Z., and R. Guicherit, Effects of stratospheric ozone depletion and tropospheric pollution on UVB radiation in

19　　the troposphere, *Photochemistry and Photobiology*, *66* (3), 346-355, 1997.

20　Madronich, S., Photodissociation in the atmosphere 1. Actinic flux and the effects of ground reflections and clouds,

21　　*Journal of Geophysical Research*, *92* (D8), 9740-9752, 1987.

22　Madronich, S., UV radiation in the natural and perturbed atmosphere, in Environmental Effects of UV (Ultraviolet)

23　　Radiation, edited by M. Tevini, pp. 17–69, A. F. Lewis, New York, 1993.

24　Madronich, S., and S. Flocke, The role of solar radiation in atmospheric chemistry, in *Environmental*

25　　*Photochemistry*, edited by P. Boule, pp. 1-26, Springer-Verlag, Berlin, 1999.

26　Nack, M.L., and A.E.S. Green, Influence of clouds, haze, and smog on the middle ultraviolet reaching the ground,

27　　*Applied Optics*, *13* (2405-2415), 2405-2415, 1974.

28　Neckel, H., and D. Labs, The Solar-Radiation between 3300-a and 12500-A, *Solar Physics*, *90* (2), 205-258, 1984.

Olson, J.R*., et al.*, Seasonal differences in the photochemistry of the South Pacific: A comparison of observations and model results from PEM-Tropics A and B, *J. Geophys. Res.*, *106* (D23), 32,749-32,766, 2001.

Papayannis, A*., et al.*, Role of urban and suburban aerosols on solar UV radiation over Athens, Greece, *Atmospheric Environment*, *32* (12), 2193-2201, 1998.

Pfister, G., D. Baumgartner, R. Maderbacher, and E. Putz, Aircraft measurements of photolysis rate coefficients for ozone and nitrogen dioxide under cloudy conditions, *Atmospheric Environment*, *34* (23), 4019-4029, 2000.

Reuder, J., and H. Schwander, Aerosol effects on UV radiation in nonurban regions, *J. Geophys. Res.*, *104* (D4), 4065-4078, 1999.

Sander, S.P.et al., Chemical kinetics and photochemical data for use in stratospheric modeling, *JPL Publ., 00-003*, 2000.

Schafer, J.S., T.F. Eck, B.N. Holben, P. Artaxo, M. Yamasoe, and A.S. Procopio, Observed reductions of total solar irradiance by biomass-burning aerosols in the Brazilian Amazon and Zambian Savanna, *Geophysical Research Letters*, *29* (17), 1823, doi:10.1029/2001GL014309, 2002.

Seckmeyer, G., R. Erb, and A. Albold, Transmittance of a cloud is wavelength dependent in the UV range, *Geophys. Res. Lett.*, *23* (20), 2753-2756, 1996.

Shetter, R.E., and M. Müller, Photolysis frequency measurements using actinic flux spectroradiometry during the PEM-Tropics mission: Instrumentation description and some results, *Journal of Geophysical Research*, *104* (D5), 5647-5661, 1999.

Shetter, R.E., L. Cinquini, B.L. Lefer, S.R. Hall, and S. Madronich, Comparison of airborne measured and calculated spectral actinic flux and derived photolysis frequencies during the PEM Tropics B mission, *Journal of Geophysical Research*, *107*, doi:10.1029/2001JD001320, 2002.

Shetter, R.E*., et al.*, Photolysis Frequency of NO_2: Measurement and Modeling during the International Photolysis Frequency Measurement and Modeling Intercomparison (IPMMI), *Journal of Geophysical Research, in press*, 2003.

Tang, Y*., et al.*, Impact of Clouds and Aerosols on Photolysis Frequencies and Photochemistry during TRACE-P, Part II: Three-dimensional study using a regional chemical transport model, Journal of Geophysical Research, submitted, 2003.

1   Thompson, A.M., The effect of clouds on photolysis rates and ozone formation in the unpolluted troposphere,

2   *Journal of Geophysical Research*, *89* (D1), 1341-1349, 1984.

3   U.S. Standard Atmosphere, 1976, U.S. Government Printing Office, Washington, D.C., 1976.

4   van Hoosier, M.E., J.-D. Bartoe, G.E. Brueckner, and D.K. Printz, Solar irradiance measurements 120 - 400 nm

5   from Space Lab-2, in *IUGG Assembly*, Vancouver, 1987.

6   van Weele, M., and P.G. Duynkerke, Effect of Clouds on the Photodissociation of NO2 - Observations and

7   Modeling, *Journal of Atmospheric Chemistry*, *16* (3), 231-255, 1993.

8   Vilà-Guerau de Arellano, J., P.G. Duynkerke, and M. van Weele, Tethered-balloon measurements of actinic flux in

9   a cloud-capped marine boundary layer, *J. Geophys. Res.*, *99* (D2), 3699-3706, 1994.

10 Weihs, P., and A.R. Webb, Accuracy of spectral UV model calculations .1. Consideration of uncertainties in input

11   parameters, *Journal of Geophysical Research-Atmospheres*, *102* (D1), 1541-1550, 1997a.

12 Weihs, P., and A.R. Webb, Accuracy of spectral UV model calculations .2. Comparison of UV calculations with

13   measurements, *Journal of Geophysical Research-Atmospheres*, *102* (D1), 1551-1560, 1997b.

14 Wendisch, M., S. Mertes, A. Ruggaber, and T. Nakajima, Vertical profiles of aerosol and radiation and the influence

15   of a temperature inversion: Measurements and radiative transfer calculations, *Journal of Applied*

16   *Meteorology*, *35* (10), 1703-1715, 1996.

17

Table 1. Selected optical properties of aerosol profiles at a relative humidity of 80% and wavelength of 550 nm for Boundary Layer (BL), Free Troposphere (FT) and Stratosphere (ST).

Profile Name	Layer	Altitude Range (km)	Optical Depth	Single Scattering Albedo	Asymmetry parameter	Angstrom Coefficient (350-500 nm)	Reference
Elterman	BL	0-2	0.249	0.99 / 0.85	0.60	1.00	*Elterman* [1968]
	FT	2-12	0.092	0.99 / 0.85	0.60	1.00	
	ST	12-50	0.039	0.99 / 0.85	0.60	1.00	
	Total		0.380				
Maritime Tropical	BL	0-2	0.038	0.998	0.774	0.07	*Hess et al.* [1998]
	FT	2-12	0.013	0.934	0.733	1.21	
	ST	12-50	0.005	1.000	0.733	0.74	
	Total		0.056				
Urban	BL	0-2	0.625	0.817	0.689	1.14	*Hess et al.* [1998]
	FT	2-12	0.013	0.934	0.733	1.21	
	ST	12-50	0.005	1.000	0.733	0.74	
	Total		0.643				

Table 2. Geographical parameters of P-3B and DC-8 aircraft profiles used in case studies.

	Universal Time (hh:mm)	Local Sun Time (hh:mm)	Latitude (deg)	Longitude (deg)	Altitude (km)	Solar Zenith Angle (deg)
P-3B Flight 17 Profile 2 27 Mar 2001						
Begin	04:18	13:55	32.93	144.26	3.227	41.21
End	04:32	14:11	32.79	144.66	0.172	43.61
DC-8 Flight 11 Profile 4 17 March 2001						
Begin	02:11	10:22	20.01	122.69	10.062	32.75
End	02:36	10:47	20.01	122.83	0.168	28.45

1   **Figure Captions:**

2   **Figure 1.** **[A]** Measured (SAFS) and cloud-free modeled (CFM) components of jNO$_2$ during

3   DC-8 flight 15 (a cloudy flight). The zenith (SAFS$_{[zenith]}$, red points) and nadir (SAFS$_{[nadir]}$, green

4   points) components of the measured jNO$_2$, as well as the total jNO$_2$ (i.e., SAFS$_{[total]}$, sum of

5   zenith and nadir components) are shown (dark blue points). Correspondingly, the CFM

6   calculated jNO$_2$ is shown for the upwelling (CFM$_{[upw]}$, brown points), the sum of direct beam

7   and downwelling diffuse (CFM$_{[dir+dwn]}$, pink points), and total (CFM$_{[tot]}$, light blue points) for the

8   same time period. **[B]** SAFS and CFM components of jO(^{1}D) during P-3B flight 17 (a relatively

9   cloud-free but highly polluted flight) using the same color symbols as described in Figure 1A

10   caption.

11   **Figure 2.** **[A]** SAFS and CFM components of jNO$_2$ during a heavily polluted profile

12   encountered on P-3B flight 17 on 27 March 2001 between 04:18 and 04:31 UT. **[B]** Comparison

13   of total jNO$_2$ for same P-3 profile as measured by SAFS (dark blue points) and modeled by CFM

14   with Maritime Tropical (light blue points), Urban (purple points), and Elterman (pink points for

15   single scattering albedo (ω) = 0.99, orange points for ω = 0.85) aerosol profiles.

16   **Figure 3.** **[A]** SAFS and CFM components of jNO$_2$ during a relatively clean air profile

17   encountered on DC-8 flight 11 on 17 March 2001 between 02:14 and 02:35 UT. Figure uses the

18   same color scheme as described in Figure 1A caption. **[B]** SAFS and CFM components of

19   jO(^{1}D) during the same DC-8 profile. **[C]** Comparison of total jNO$_2$ for same DC-8 profile as

20   measured by SAFS (dark blue points) and modeled by CFM with Maritime Tropical (light blue

21   points), Urban (purple points), and Elterman (pink points for single scattering albedo (ω) = 0.99,

22   orange points for ω = 0.85) aerosol profiles.

1   **Figure 4.** **[A]** The jNO$_2$ J-Value Impact Factor (JIF), calculated from the 1-minute merge, is

2   shown plotted as a function of altitude for all of TRACE-P. Blue and red points represent the P-

3   3B and DC-8 aircraft samples, respectively. **[B]** Stacked frequency distribution of the jNO$_2$ JIF

4   for the combined TRACE-P (DC-8 and P-3B) dataset with red, green, and blue bars representing

5   0 to 1 km, 1 to 5 km, and 5 to 12 km altitude bins, respectively. **[B, inset]** Cloud impacts

6   experienced during TRACE-P shown as a percent of mission in "cloud-free", reduced UV, and

7   enhanced UV conditions for each of the three altitude bins described in Figure 4B.

8   **Figure 5.** **[A]** The ratio of the steady-state (SS) OH concentration determined using the SAFS

9   photolysis frequencies ([OH]$_{SAFS}$) to the SS [OH] calculated with the CFM j-values ([OH]$_{CFM}$) as

10   a function of the jO(^{1}D) j-value impact factor (JIF) for the combined TRACE-P dataset. Red,

11   green, and blue points correspond to aircraft samples collected in 0 to 1 km, 1 to 5 km, and 5 to

12   12 km altitude bins, respectively. **[B]** The [HO$_2$]$_{SAFS}$ to [HO$_2$]$_{CFM}$ ratio versus jO(^{1}D). **[C]** The

13   [H$_2$O$_2$]$_{SAFS}$ to [H$_2$O$_2$]$_{CFM}$ ratio as a function of the jO(^{1}D) JIF. **[D]** The [NO]$_{SAFS}$ to [NO]$_{CFM}$

14   ratio as a function of the jNO$_2$ JIF. **[E]** The [NO$_2$]$_{SAFS}$ to [NO$_2$]$_{CFM}$ ratio as a function of the

15   jNO$_2$ JIF. **[F]** The [HCHO]$_{SAFS}$ to [HCHO]$_{CFM}$ ratio as a function of the jNO$_2$ JIF. **[G]** The

16   [PAN]$_{SAFS}$ to [PAN]$_{CFM}$ ratio as a function of the jNO$_2$ JIF. **[H]** The [CH$_3$C(O)O$_2$]$_{SAFS}$ to

17   [CH$_3$C(O)O$_2$]$_{CFM}$ ratio as a function of the jNO$_2$ JIF.

18   **Figure 6.** The calculated fraction of NO$_X$ that is present as NO$_2$ for the combined TRACE-P

19   dataset, plotted as a function of altitude for both the SAFS (black) and CFM (red) photolysis

20   frequencies.

21   **Figure 7.** **[A]** The ratio of the calculated instantaneous ozone production rate determined using

22   the SAFS photolysis frequencies (O$_3$ production $_{[SAFS]}$) to the instantaneous ozone production

23   rate calculated with the CFM j-values (O$_3$ production $_{[CFM]}$) as a function of the jNO$_2$ j-value

1   impact factor (JIF) for the combined TRACE-P dataset. Red, green, and blue points correspond

2   to aircraft samples collected in 0 to 1 km, 1 to 5 km, and 5 to 12 km altitude bins, respectively.

3   **[B]** The instantaneous ratio of "O_3 loss $_{[SAFS]}$" to "O_3 loss $_{[CFM]}$" versus the JIF. **[C]** The

4   instantaneous ratio of "net O_3 tendency $_{[SAFS]}$" to "net O_3 tendency $_{[CFM]}$" versus the JIF. Dotted

5   lines are the 99% confidence interval for this linear regression.

6   **Figure 8.** The average rate of O_3 production, O_3 loss, and the net O_3 tendency (production –

7   loss) for all samples in 0-1 km, 1-5 km, and 5-12 km altitude bins for both the SAFS (blue) and

8   CFM (red) photochemical box model runs.
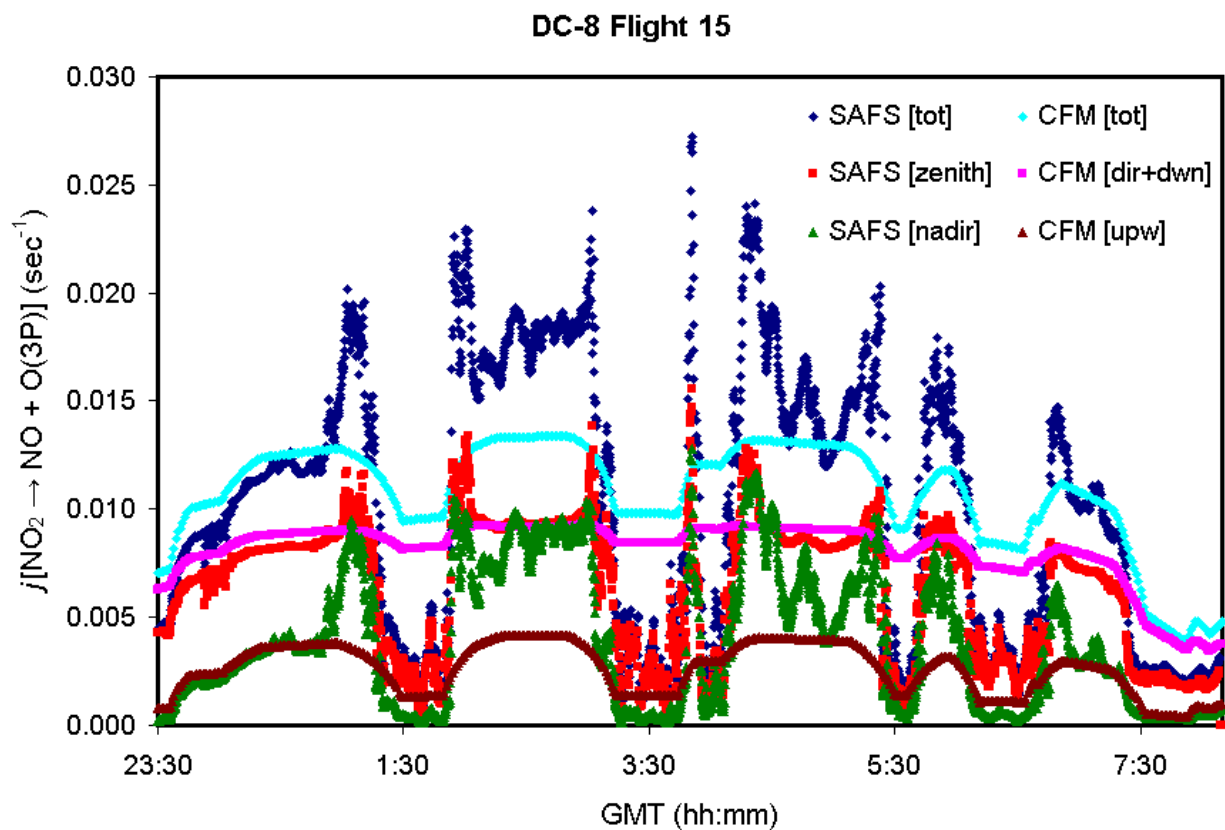
Figure 1A.
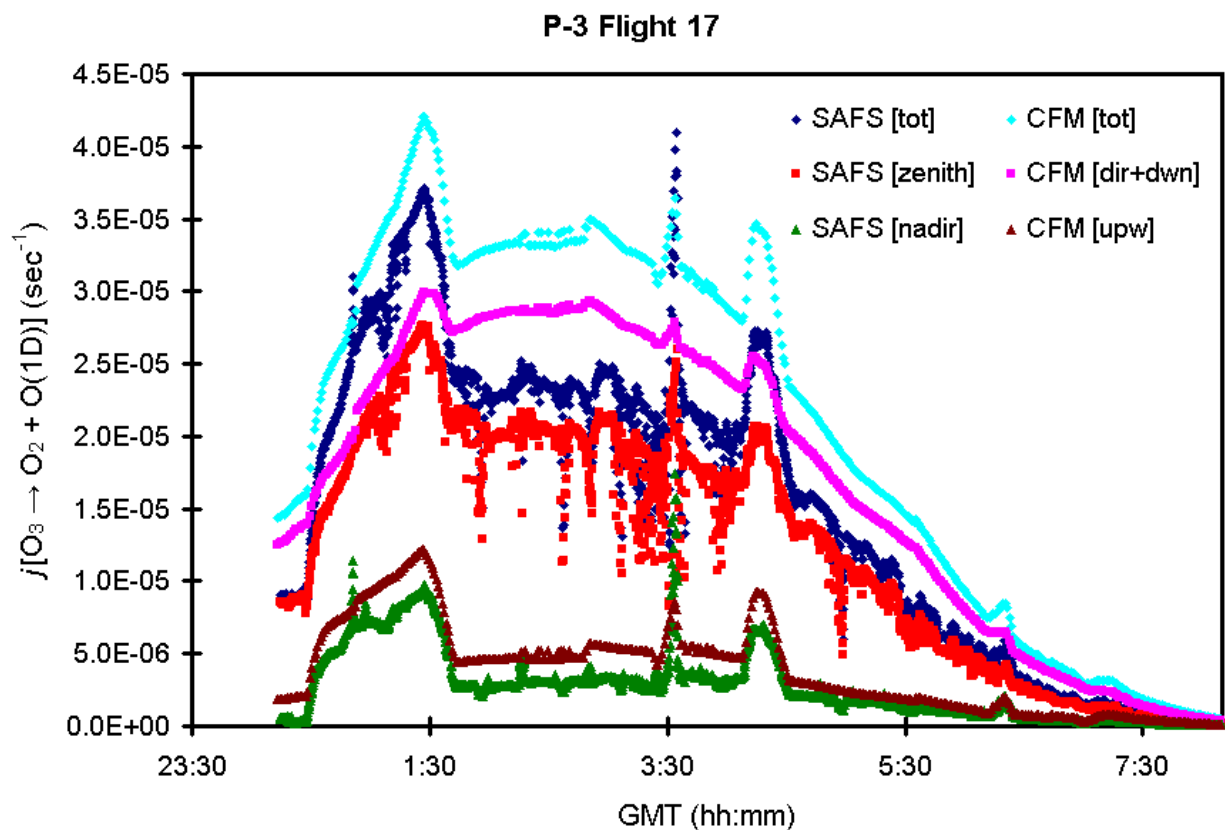
Figure 1B.
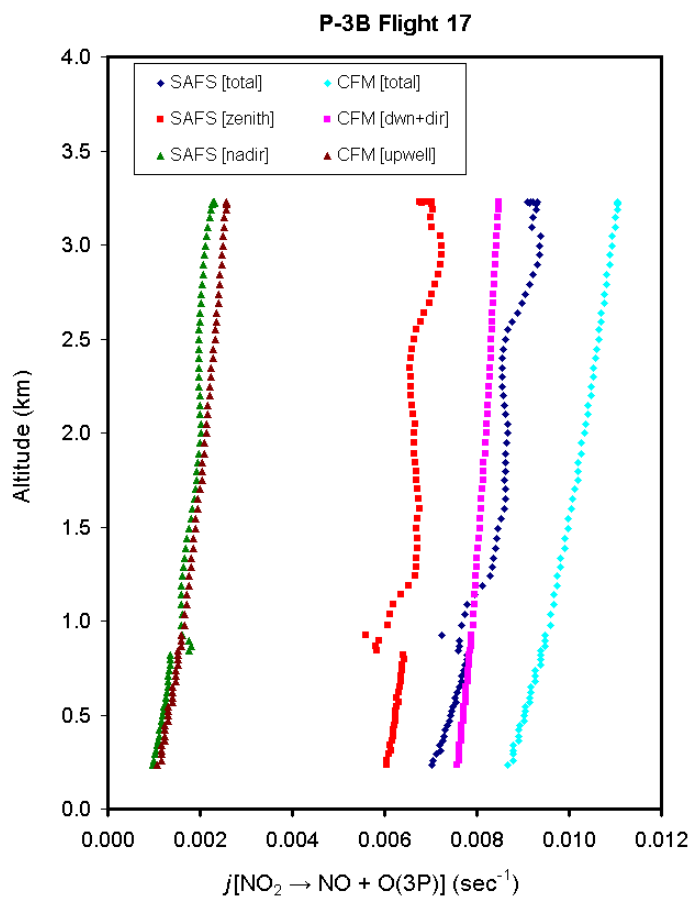
Figure 2A.
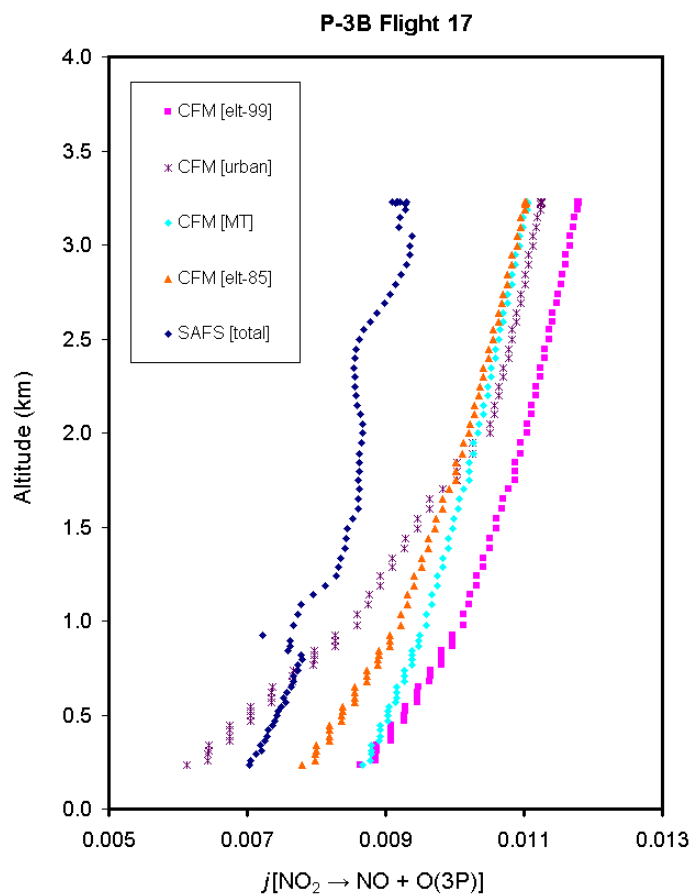
Figure 2B.

DC-8 Flight 11
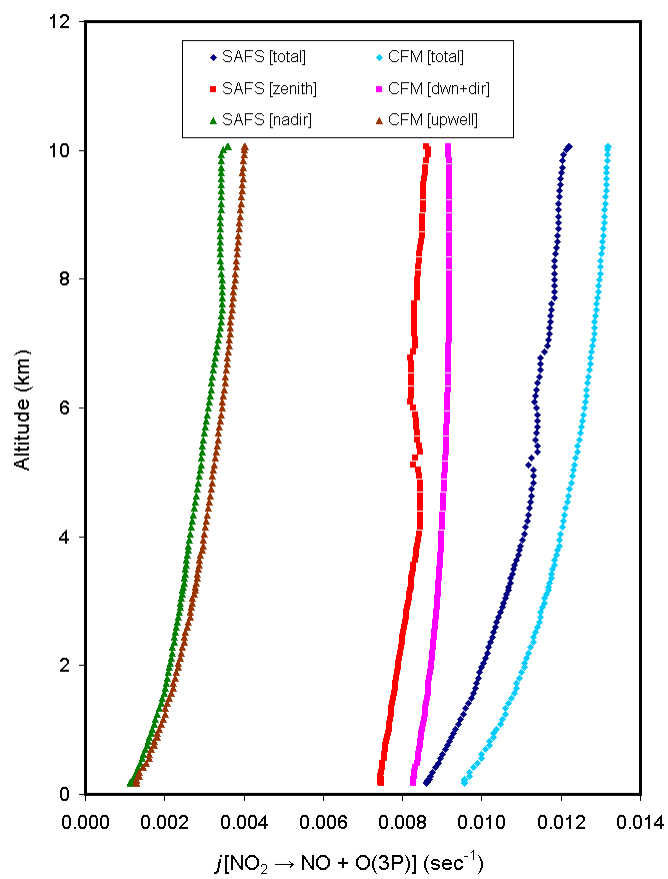
Figure 3A.

DC-8 Flight 11

Figure 3B.

DC-8 Flight 11
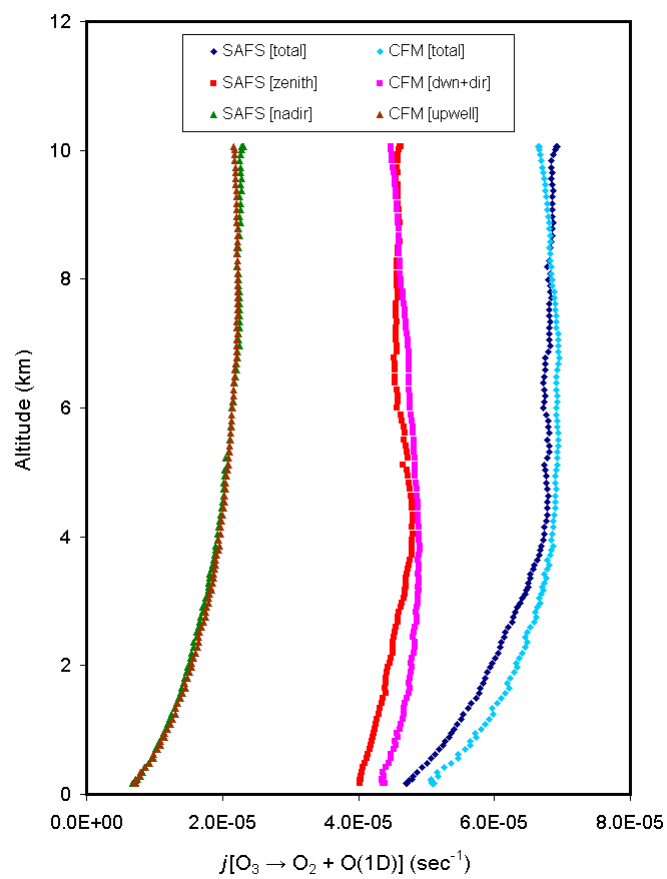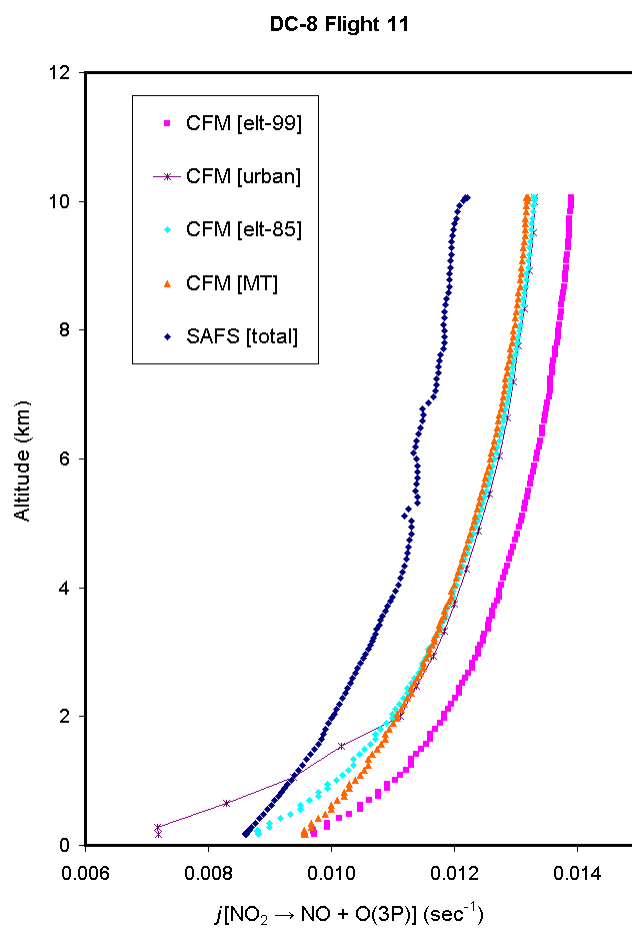
Figure 3C.

Figure 4A

Figure 4B

$$y = 0.894x + 0.072$$
$$r^2 = 0.948$$

Figure 5A.

$$y = 0.991 \, x^{0.525}$$
$$r^2 = 0.975$$
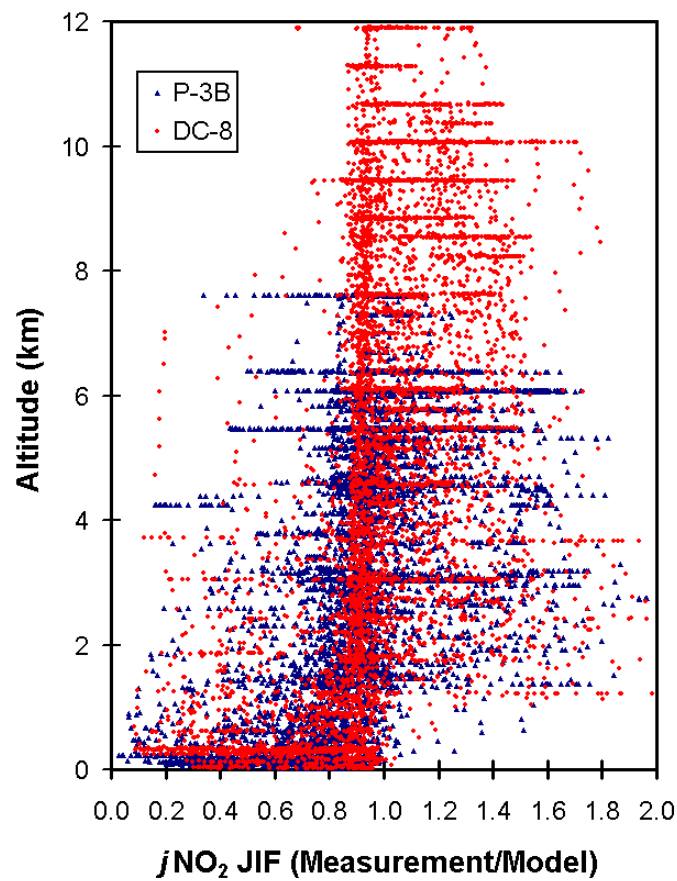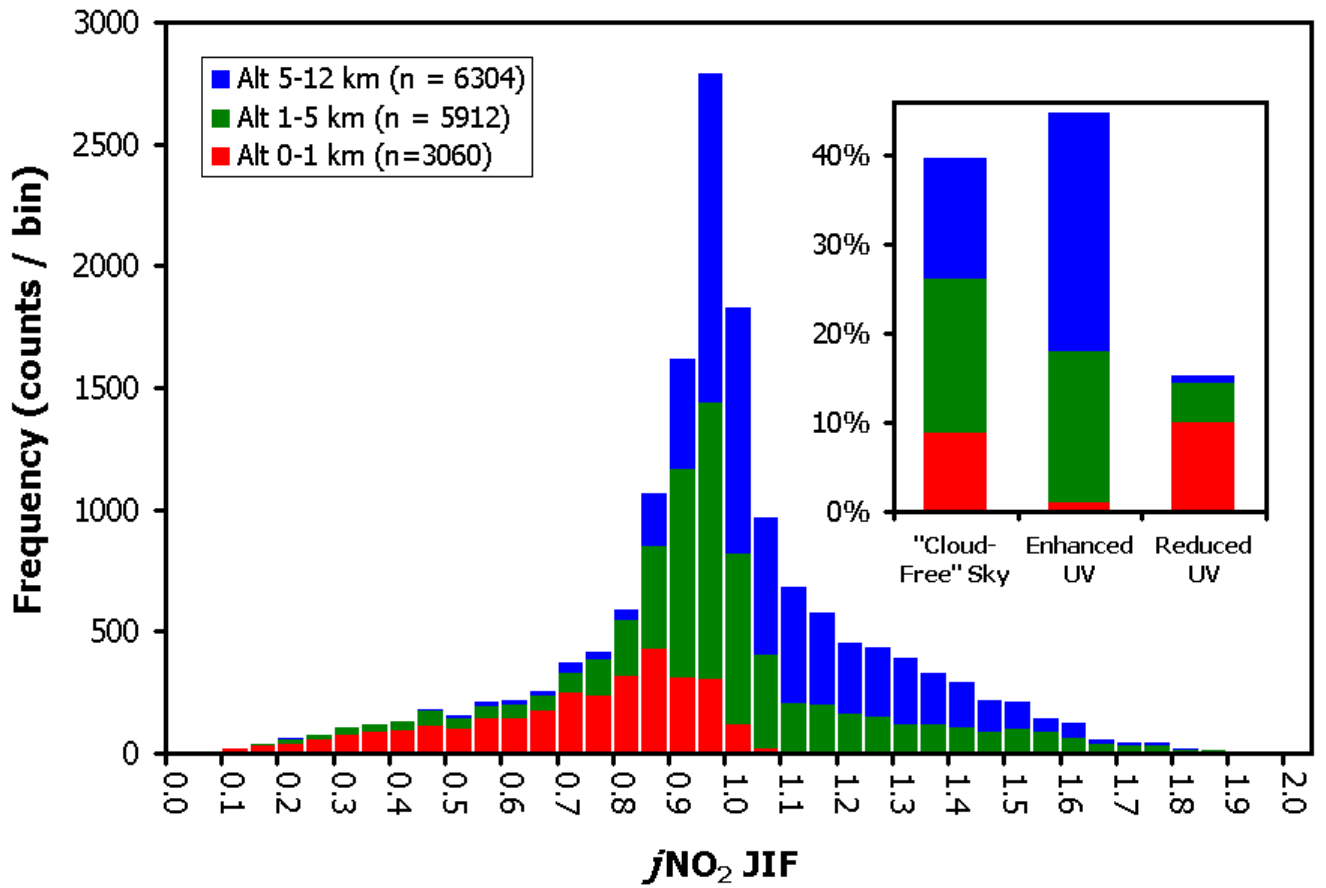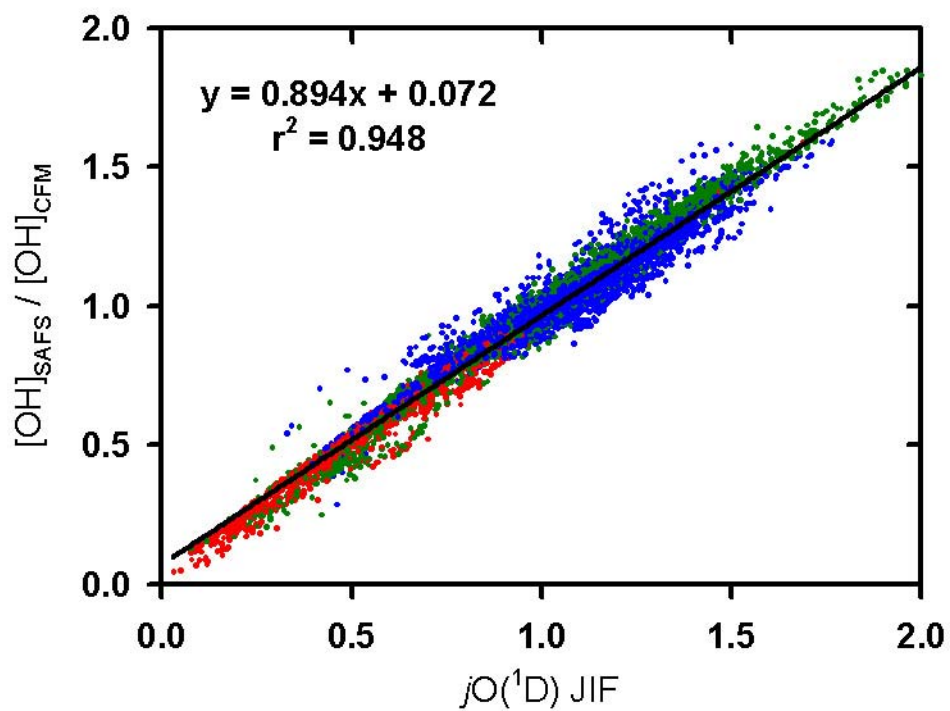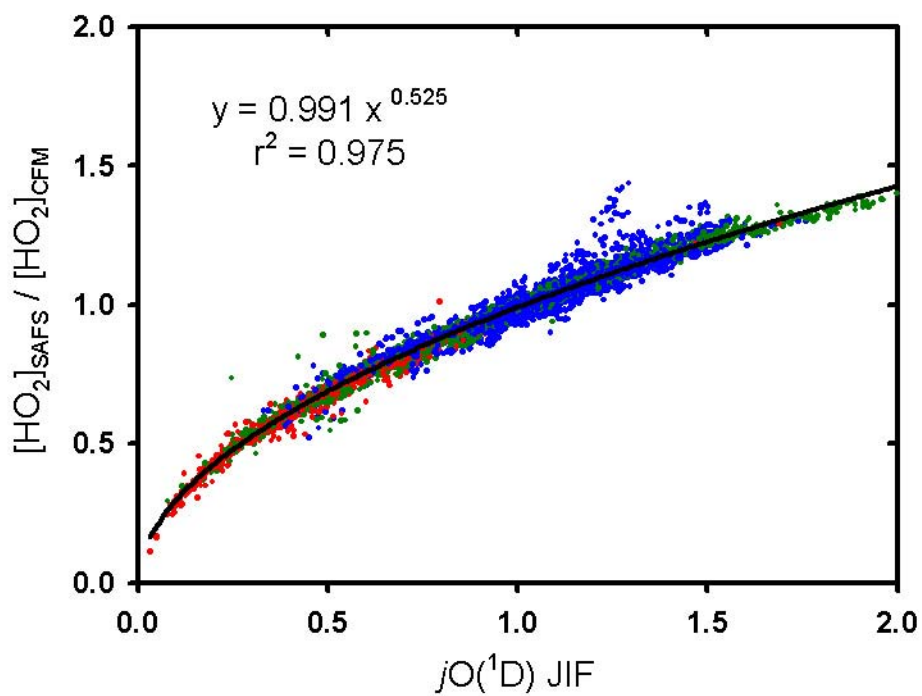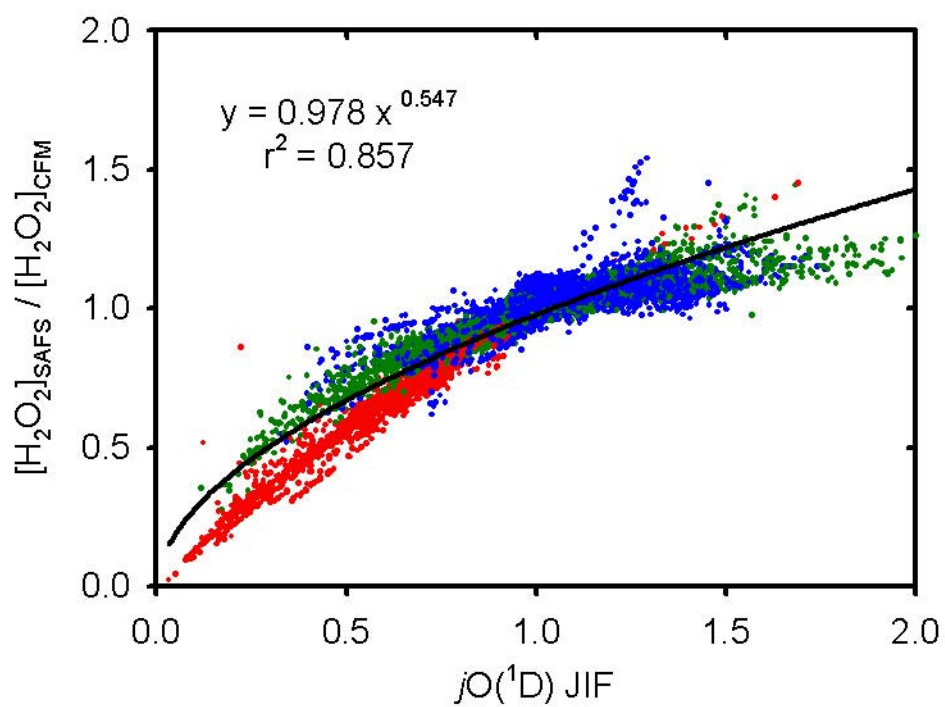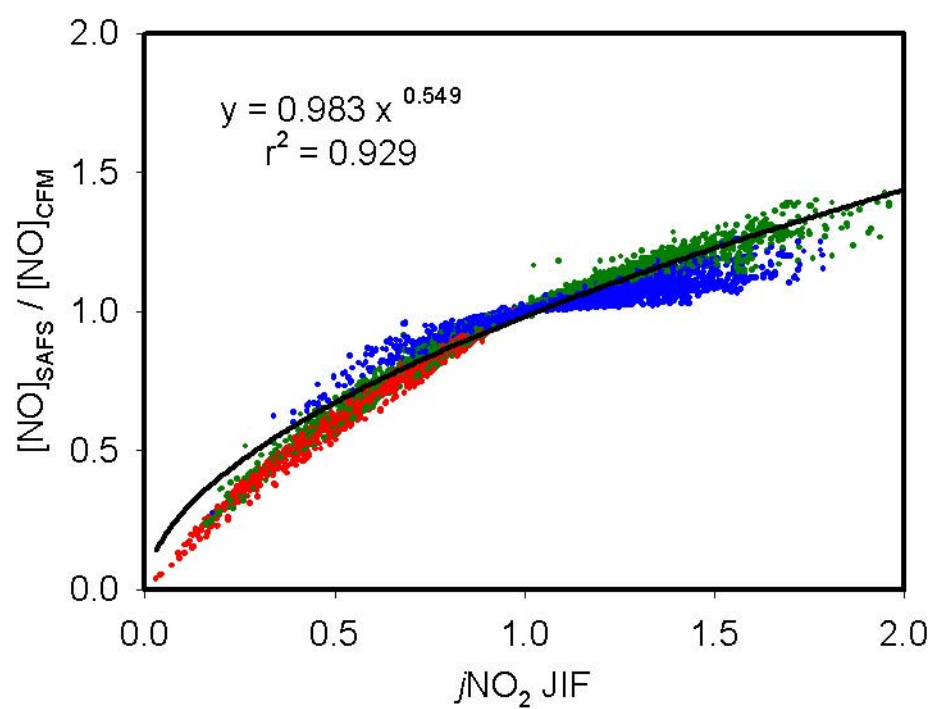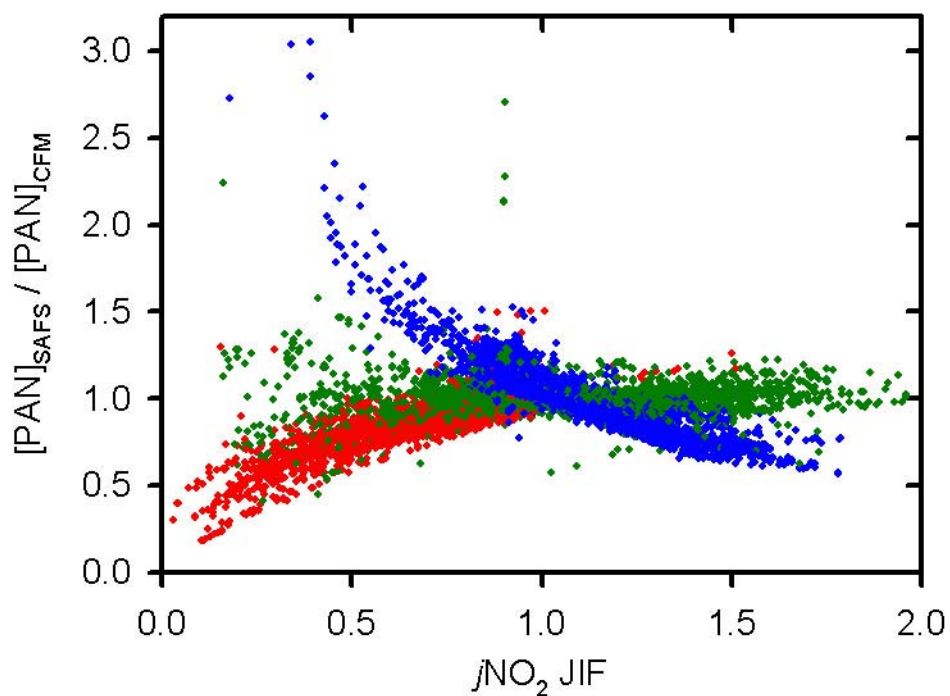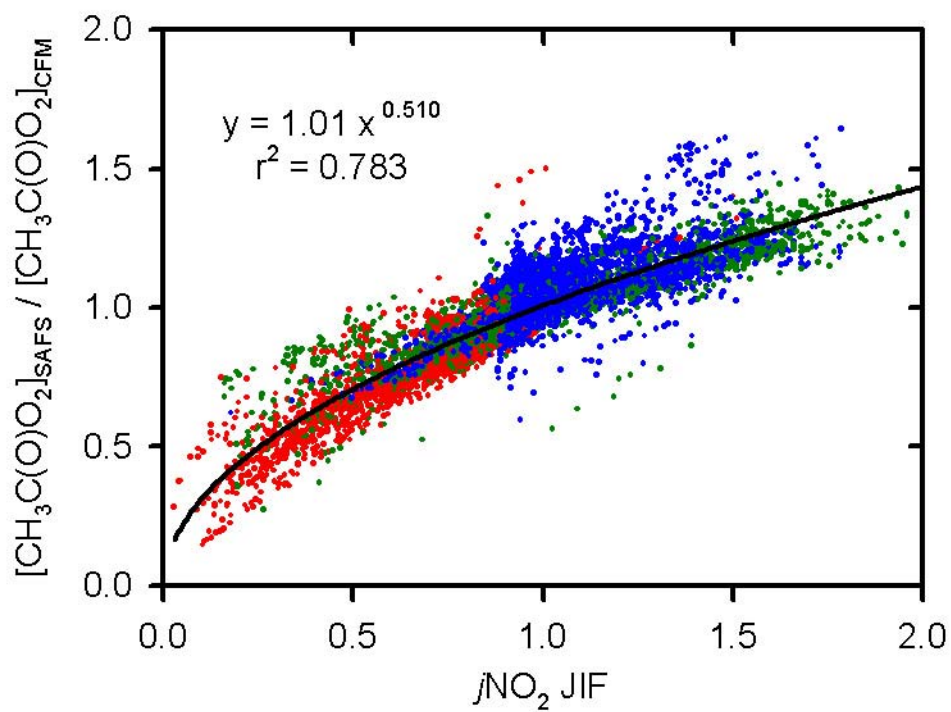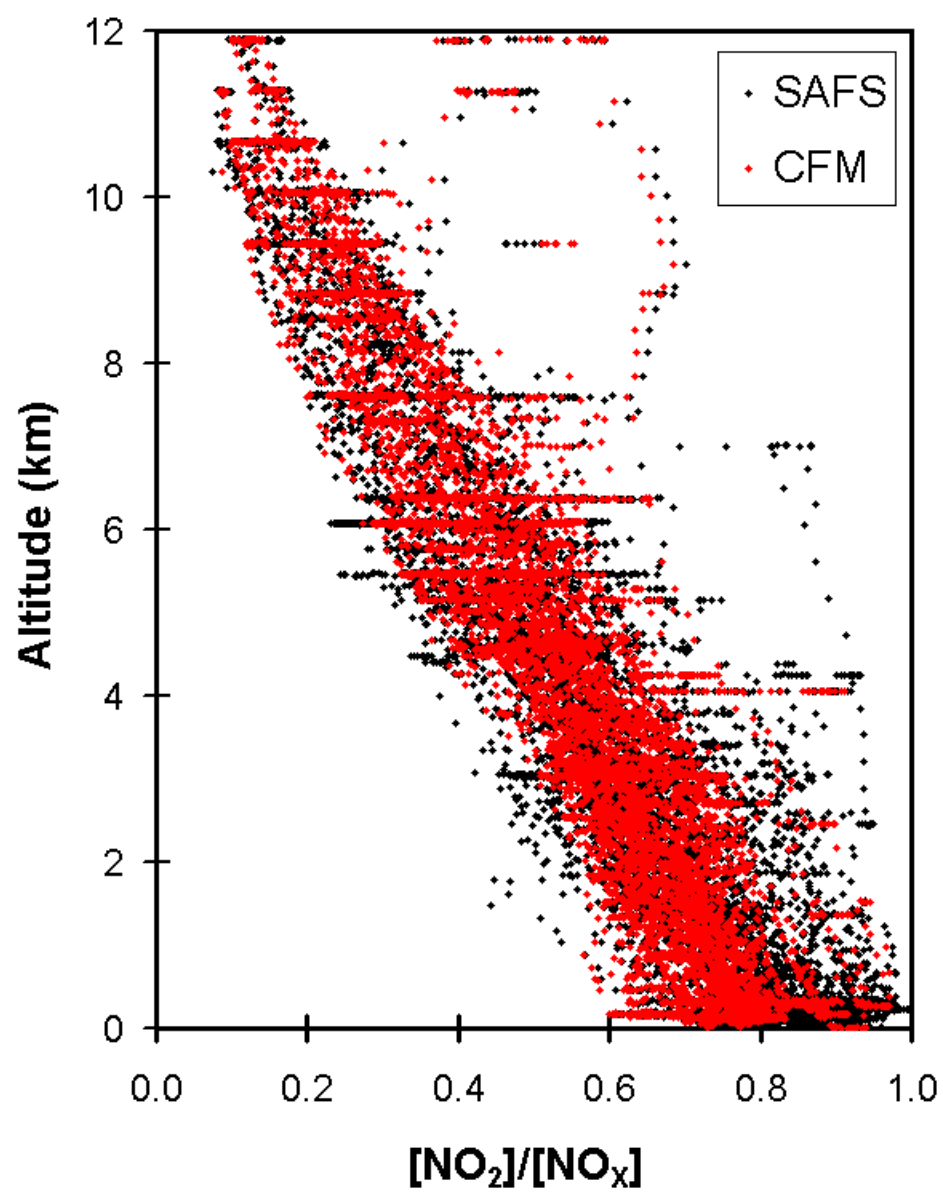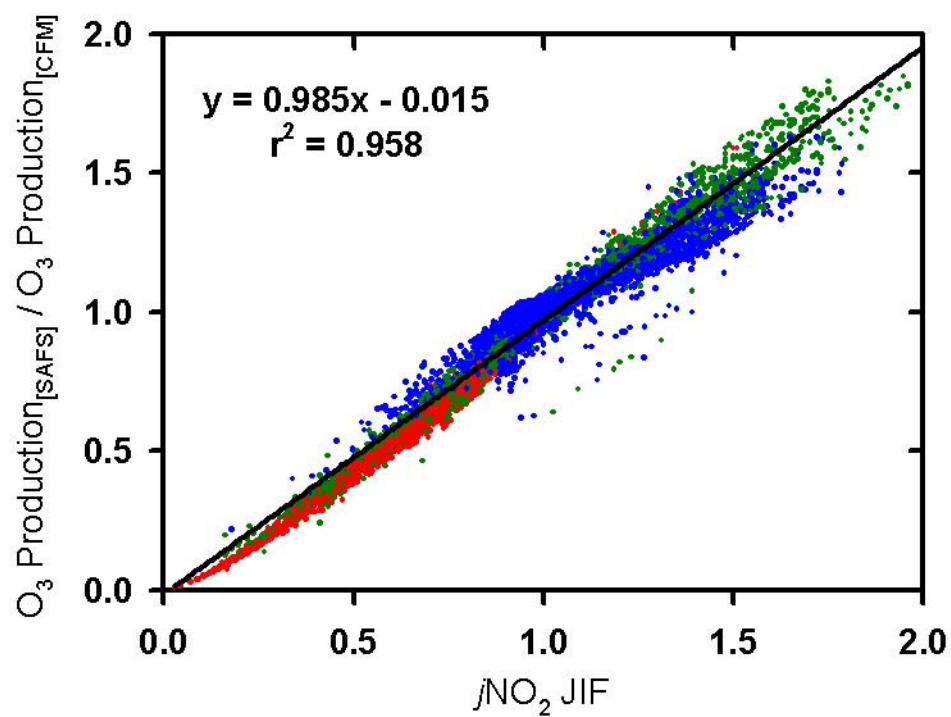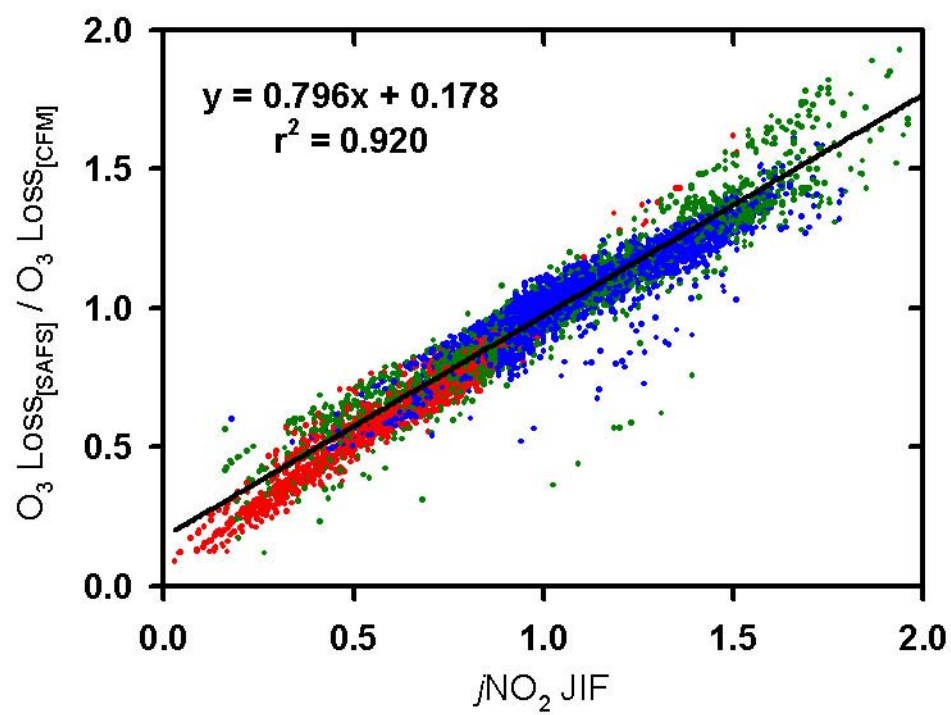
Figure 5B.

Figure 5C.

Figure 5D.
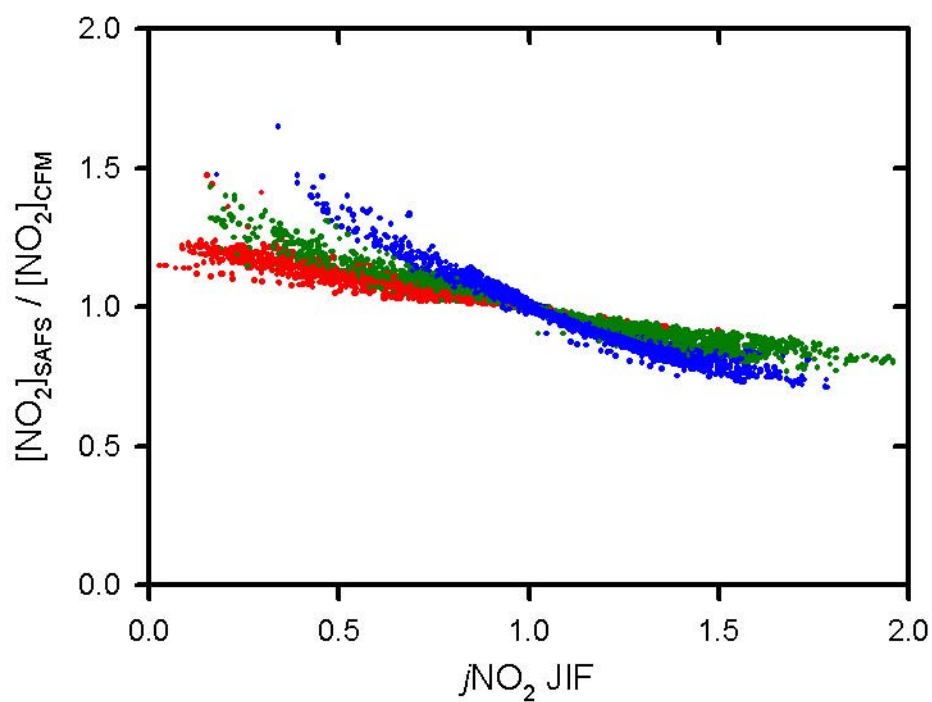
Figure 5E.
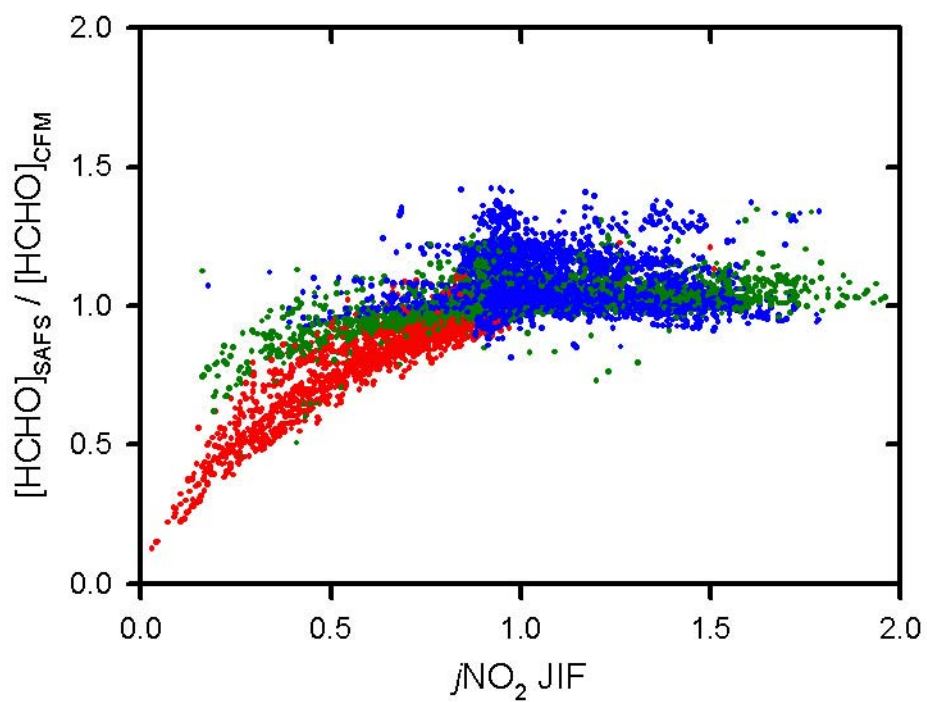
Figure 5F.

Figure 5G.

Figure 5H.

Figure 6.

Figure 7A.

Figure 7B.

$$y = 0.947x + 0.008$$
$$r^2 = 0.077$$

Figure 7C.

Figure 8.